Uncertainty assessment of drought characteristics projections in humid subtropical basins in China based on multiple CMIP5 models and different index definitions

Kai Xu[a], Chuanhao Wu[a,b*], Ce Zhang[c,d], Bill X. Hu[a,b]

[a] *Institute of Groundwater and Earth Sciences, Jinan University, Guangzhou 510632, China*

[b] *Green Development Institute of Zhaoqing, Zhaoqing, China*

[c] *Lancaster Environment Centre, Lancaster University, Lancaster LA1 4YQ, United Kingdom*

[d] *UK Centre for Ecology & Hydrology, Library Avenue, Bailrigg, Lancaster LA1 4AP, United Kingdom*

Author for correspondence

Chuanhao Wu (wuch0907@jnu.edu.cn)

Institute of Groundwater and Earth Sciences, Jinan University, Guangzhou 510632, China.

Abstract

This study presents an assessment of projection and uncertainty of drought characteristics (frequency D_F, drought area Da) using three drought indices (Palmer Drought Severity Index, PDSI; Standardized Precipitation Index, SPI; Standardized Precipitation Evapotranspiration Index, SPEI) in the humid subtropical Pearl River basin in southern China during the period 2021-2050. The projection is based on 13 CMIP5 general circulation models (GCMs) under three Representative Concentration Pathway scenarios (RCP2.6, RCP4.5 and RCP8.5). Specifically, the SPI is derived by the precipitation simulations of 13 GCMs, whereas the PDSI and SPEI are computed based on the simulations from the Variable Infiltration Capacity (VIC) model forced by 13 GCMs. The uncertainty of projected drought indices (PDSI, SPI and SPEI) due to various GCMs and RCPs is quantified by the variance-based sensitivity analysis approach. The results indicate that the sign and magnitude of the projected changes in D_F and Da are highly dependent on the index definition at the regional scale, and the SPI tends to underestimate the projected changes in D_F compared with PDSI and SPEI. There is a large model spread in the projected D_F changes (especially for SPEI) under all RCP scenarios, with larger model spread for more extreme drought events. Uncertainty analysis shows that GCM contributes more than 90% of total uncertainty in drought indices projections, while the RCP uncertainty is rather limited (< 10%) compared with GCM. The GCM uncertainty is spatially unevenly distributed and shows large variability at the interannual scale. This study highlights the sensitivity of drought projections to the index definition as well as the large spatial-temporal variability of general sources of uncertainty in drought projections.

Key words: Drought projection; Drought indices; uncertainty quantification; CMIP5; RCPs

1. Introduction

Drought is a stochastic and recurring natural hazard that has devastating impacts on economy, society, and ecosystem services around the word (Piao et al., 2010; Dai, 2011a; Thornton et al., 2014; von Buttlar et al., 2018). The economic loss caused by drought hazards is enormous, with an annual loss estimate of \$6~8 billion at a global scale (Wilhite, 2000). The Intergovernmental Panel on Climate Change (IPCC)'s 4th and 5th Assessment Report (AR4 and AR5) indicated that global surface mean temperature (T) is likely to increase 0.3~4.8°C, accompanied by changes in spatial patterns and intensity of precipitation (P) by the end of this century (IPCC, 2007; 2013). Global warming is expected to exacerbate extreme events such as droughts, leading to significant changes in area and intensity of drought all around the world (Dai, 2013; Cook et al., 2014; Trenberth et al., 2014; Gudmundsson et al., 2017; Samaniego et al., 2018). Exploring projected changes in drought intensity and frequency under various emission scenarios can help prepare for future disaster prevention and mitigation, and support sustainable development.

Drought is an abnormal phenomenon that can occur in short periods (days and weeks) or long periods (months or longer), and can commonly be characterized by drought monitoring indices. Typically, droughts are classified into four major types: meteorological drought, hydrological drought, agricultural drought, and socioeconomic drought (Heim, 2002; AMS, 2004; Hayes et al., 2011; Mishra and Singh, 2011). Different types of drought have distinct spatiotemporal characteristics, and they vary at different scales (Peters et al., 2006; Tallaksen et al., 2009). Meteorological drought is identified by a prolonged lack of P as the main indicator, resulting in total soil moisture (SM) deficits (i.e., agricultural drought) as well as the decrease of streamflow, groundwater, reservoir and lake levels (i.e., hydrological drought). Such drought hazards can also lead to severe consequence of drinking water scarcity, and negatively impact crop yield and production, and result in economic loss. Socioeconomic definitions of drought associate the supply and demand of certain economic good with elements of meteorological, agricultural and hydrological drought (Wilhite and Glantz, 1985).

In the past decades, numerous indices have been proposed to quantify the drought and wet conditions based on different hydroclimatic variables (e.g., *T*, *P,* evapotranspiration *ET*, *SM* and runoff *RO*), of which the most commonly used is the Palmer Drought Severity Index (PDSI; Palmer, 1965), the Rainfall Anomaly Index (RAI; van Rooy, 1965), the Crop Moisture Index (CMI; Palmer, 1968), the Soil Moisture Drought Index (SMDI; Hollinger et al., 1993), the Surfacewater Supply Index (SWSI; Shafer and Dezman, 1982), the Standardized Precipitation Index (SPI; Mckee et al., 1993, 1995), the Standardized Runoff Index (SRI; Shukla and Wood, 2008), the Standardized Precipitation Evapotranspiration Index (SPEI; Vicente-Serrano et al., 2010), and the aridity index (AI; Huang et al., 2016). The use of different types of drought indices often leads to different spatio-temporal variabilities of drought characteristics, even though they are calculated using the inputs of hydroclimatic variables generated by the same modeling system (Burke and Brown, 2008; Ukkola et al., 2018). For example, PDSI and SPEI can measure the warming effect more explicitly through enhanced *ET* than other drought indices based on *P* alone (e.g., SPI).

The General Circulation Models (GCMs), released by the Coupled Model Intercomparison Project (CMIP), are the primary tools for estimating trends and variability of future climate change (IPCC, 2007; 2013). Based on GCM simulations, the influence of climate change on droughts have been investigated by numerous studies. The majority of research indicated an increased drought risks over different regions globally as the level of greenhouse gas (GHG) emission increases (e.g., Wang, 2005; Sheffield and Wood, 2008; Li et al., 2012; Dai, 2011b, 2013; Cook et al., 2014; Wang and Chen, 2014; Rhee and Cho, 2016; Wu et al., 2016; Zhao and Dai, 2017; Ruosteenoja et al., 2018; Wang et al., 2018; Amnuaylojaroen et al., 2019; Rudd et al., 2019). Although enormous efforts have been made to project how the drought risk would occur as the result of GHG emission increase, few studies have assessed and quantified the source of uncertainty in projecting future drought conditions. This uncertainty is due mainly that drought is a complex process coupled with multiple meteorological factors (e.g., *P* and *ET*), as well as various geomorphic and topographic characteristics of specific regions. These key factors are described differently amongst GCMs, which form the main source of uncertainty resulting in the lack of consistency between model projections (Wang et al., 2018; Lee et al., 2019; Xu et al., 2019b; Wu et al., 2021).

This research focuses on Pearl River as the third longest River in China and composed of West River, North River, East River, and Pearl River Delta. Pearl River is an important source of fresh water for large cities in the Guangdong-Hong Kong-Macao Greater Bay Area, such as Guangzhou, Zhuhai, Hong Kong and Macau (Zhang et al., 2008). The Pearl River basin (PRB) is climatically humid with abundant *P*, but the spatiotemporal distribution of *P* is uneven across the basin, with frequent extreme weather events, such as floods and droughts. In recent years, the PRB has suffered from droughts considerably with large severity and prolonged periods of water deficit, presenting severe droughts events such as in 2004, 2005, 2010 and 2011 (Zhang et al., 2012; Zhang et al., 2015; Wu et al., 2016; Chen et al., 2017; Xu et al., 2019a).

The temporal and spatial evolution of drought characteristics in the PRB has been analyzed by several drought metrics (e.g. Zhang et al., 2009; Zhang et al., 2012; Fischer et al., 2013; Niu et al., 2015; Xiao et al., 2016; Xu et al., 2019a). Recently, several studies have projected changes in drought characteristics in the PRB under future climate scenarios using CMIP5 models (Wu et al., 2016; Wang et al., 2018). For example, Wang et al. (2018) predicted the spatiotemporal changes in future drought in PRB using the PDSI and CMIP5 GCM simulations, and found that the severity of drought would likely to be increased in the central and western regions of the PRB. However, these studies were based solely on one drought index and a few models. Previous research has reported that the sign and magnitude of projected drought is highly dependent on the selection of drought index, region, and model ensemble (Burke and Brown, 2008; Rhee and Cho, 2016; Ahmadalipour et al., 2017; Ukkola et al., 2018; Lee et al., 2019). More importantly, general sources of uncertainty (e.g., GCMs and RCP scenarios) in drought projection have not been explored in the PRB, and hence our knowledge on uncertainties and their spatial and temporal variability in GCM-projected drought remains limited at the basin scale.

To address this gap, our research presents a basin-scale assessment of future drought characteristics projections in the PRB (including the West River and North River) by using 13 CMIP5 GCMs, three RCP scenarios (RCP2.6, RCP4.5 and RCP8.5), and three different drought indices (PDSI, SPI and SPEI). Specifically, an advanced hierarchical sensitivity analysis is conducted to quantify the uncertainties in the projection of three drought indices (PDSI, SPI and SPEI) due to three RCP scenarios and 13 GCMs at both spatial and temporal scales. The objectives of this study are (1) to test the sensitivity of projection of future drought characteristics with respects to index definition and various model ensemble members and (2) to explore the spatio-temporal variability of uncertainties of GCM and RCP, and rank the contribution of each uncertainty to the projections of drought indices. In Section 2, detailed information on the observed and modeling datasets for the study area, and the methods for bias correction, hydrological modeling, drought indices and uncertainty estimation used in this study are provided. Followed by the results and discussion presented in Sections 3 and 4, respectively. Finally, the conclusions are drawn in Section 5.

2. Study area and data source

2.1 Study area

The Pearl River, located in southern China, is the third largest River in drainage basin area in China (Fig.1). It consists of the West River, North River and East River as well as the Rivers within the Pearl River delta. The water resources are unevenly distributed spatially over the PRB and are mainly concentrated in the West River and North River basins, account for approximately 93.7% of the total area of the PRB (Zhang et al., 2013a). The PRB is characterized by tropical and subtropical climate zones, with mean annual *T* ranging from 14 to 22 °C and mean annual *P* of approximately 1525 mm (Zhang et al. 2012; Wu et al. 2013). The *P* over the PRB is mainly concentrated in the flooding season between April and September, covering 80% of the total annual *P* (Zhang et al. 2012). Due to climate warming, the hydrological cycle has become more changeable over the PRB in recent years, resulting in an increased risk of extreme flooding and drought (e.g., droughts in 2004, 2005, 2010, and 2011), influence significantly on agriculture and ecological environment, and causing disastrous damage to human lives and social economy.

2.2 Data sources and processing

2.2.1 Meteorological and hydrological observations

In this study, the observed data of meteorology and hydrology from 1971 to 2000 were collected for analysis. The daily data of *P*, maximum/minimum *T*, and wind speed were obtained from 57 meteorological stations (Fig.1) over the PRB as provided by the National Meteorological Information Center (NMIC) of China Meteorological Administration (http://data.cma.cn). For quality control of the observed data, we checked any cases of maximum *T* less than minimum *T* or *P* values below 0 mm. The daily record of the neighboring stations were also cross-compared, which helps to check the correctness of values and any outliers. In addition, the homogeneity evaluation of data was carried out and the test indicated that the meteorological data used were free from severe errors (Wu et al., 2016). Daily runoff observations from the Gaoyao (1980-2000) and Hengshi (1970-2000) hydrological stations, in the West River and North River basins, were provided by the Hydrology Bureau of Guangdong Province, China.

2.2.2 GCM simulations

The downscaling results of the multimodel dataset of the 13 CMIP5 GCMs (Table 1) were provided by the College of Global Change and Earth System Science, Beijing Normal University. These 13 GCMs were chosen because they demonstrated well performance in simulating the spatial and temporal variability of T and P over southern China (Huang et al., 2013; Chen and Frauenfeld, 2014). The downscaling process of 13 GCMs is as follows: first, the monthly outputs of GCMs were interpolated to the sites over the Pearl River basin by using the bilinear interpolation method, and corrected by the observed data. Then the bias-corrected outputs of GCMs were weighted averaged by the Bayesian model averaging method at the site scale, and were temporally downscaled to multiple daily simulation samples (30 samples) using the stochastic weather generation method according to the four categories (hot-wet, hot-dry, cold-wet, and cold-dry) of the historical weather years. Finally, the daily simulations were interpolated onto a common 0.25° × 0.25° grid over the Pearl River basin using the bilinear interpolation method. The detailed information on the statistical downscaling process of the 13 GCMs can be found in Wu et al. (2014).

The downscaling simulations of these GCMs were used in this study, mainly because of their good performance in reproducing daily variability of T and P in the Pearl river basin (see Figures 4b and 5b in Wu et al., 2014). In addition, the multiple simulation samples of the 13 GCMs can well represent the uncertainty range of GCMs. The daily data for the baseline period 1971-2000 and the near future period 2021-2050 with three different RCPs scenarios (i.e., RCP2.6, RCP4.5 and RCP8.5) are employed. For each RCP scenario, a total of 30 simulation samples were collected to represent the uncertainty range of GCMs.

3. Methodology

3.1 Bias correction and adaptability assessment

Many studies did not use climate model outputs directly for analyzing climate change impact due to bias in GCM data (Lafon et al., 2013, Wu and Huang, 2016). In this research, a "delta change" method was adopted to correct bias in T and P data of the downscaling multi-model ensembles of 13 CMIP5 GCMs (Hay et al., 2000; Sperna Weiland et al., 2010; Wu and Huang, 2016). For T (in units of °C), an additive correction was used:

$$T_{cor,i,j} = T_{sim,i,j} + \left(\overline{T}_{obs,i,j} - \overline{T}_{sim,i,j}\right) \quad (1)$$

For P (in units of mm), a multiplicative correction was applied:

$$P_{cor,i,j} = P_{sim,i,j} \times \frac{\overline{P}_{obs,i,j}}{\overline{P}_{sim,i,j}} \quad (2)$$

where ($T_{cor,i,j}$) $P_{cor,i,j}$ and ($T_{sim,i,j}$) $P_{sim,i,j}$ are the bias-corrected and simulated ith daily T (P), respectively, for the jth grid point. $\overline{T}_{obs,i,j}$ ($\overline{P}_{obs,i,j}$) and $\overline{T}_{sim,i,j}$ ($\overline{P}_{sim,i,j}$) are the 30-year averages of the observed and simulated ith daily T (P), respectively, at the jth grid point for the baseline period 1971-2000.

3.2 VIC model

The VIC model is a macro-scale, semi-distributed hydrological model based on a grid-based land surface process scheme (Liang et al., 1994). It has the characteristics of *ET* calculation based on physical process, computation of water and energy balances simultaneously, and consideration of spatial heterogeneity in *SM* content of the grid (Liang et al., 1996). More detailed information about VIC model can be found at the University of Washington's website (http://ftp.hydro.washington.edu/Lettenmaier/Models/VIC/). As a typical land surface model, the VIC model has been successfully applied in the PRB for *SM* simulation (Niu et al., 2015) and the impact of climate change on hydrology by coupling with GCMs (e.g. Wu et al., 2014; Wu et al., 2015; Yan et al., 2015; Wang et al., 2018).

Here, the latest version VIC 5.0 model (https://vic.readthedocs.io/en/master/) was adopted to run at a spatial resolution of 0.25°×0.25° over the West and North River basins. The soil column of the model is divided vertically into three layers (top, middle and bottom), and the top and middle soil layers were considered for calculating the PDSI (Wang et al., 2018). The soil parameters were derived from the

1-km spatial resolution global soil classification and texture dataset provided by the FAO's Harmonized World Soil Database (HWSD) (FAO et al., 2009). The soil information was converted into soil hydraulic parameters based on Saxton and Rawls (2006). The land cover data were driven from the global 1-km land cover classification of the University of Maryland (Hansen et al., 2000; https://www.geog.umd.edu/landcover/1km-map.html). This dataset includes vegetation-related parameters such as architectural resistance, leaf-area index, albedo, minimum stomata resistance, and fraction of root depth of each soil layer. We assumed that the land cover of the PRB would not change significantly in the future, and the land cover data of 2000 was used for hydrological simulation over both baseline (1971-2000) and the future period (2021-2050). The VIC model provides several daily output variables for surface water fluxes calculation, including *ET*, *PET*, *SM* and runoff (*RO*). The daily simulations of VCI model were aggregated into monthly time series to compute the monthly water balance and drought indices (SPEI and PDSI).

3.3 Drought indices

3.3.1 SPI and SPEI

The SPI was originally developed to quantify the *P* deficit at multiple time-scales (Mckee et al., 1993). Although the SPI considers only *P*, it has been widely used in different meteorological, agricultural and hydrological applications thanks to its simplicity in calculation and general applicability, as well as the consistency over space and time (Hayes et al., 1999; Mishra et al., 2005; Zhang et al., 2009; Mishra and Singh, 2011; Huang et al., 2014; Zhu et al., 2016; Xu et al., 2019a). For SPI calculation, the probability distribution is used initially to fit the long-term monthly *P*, and the cumulative distribution function (CDF) is then turned into the normal distribution through equal probabilities. The gamma distribution is used in this research to describe the probability density function (PDF) of *P*:

$$g(x)=\frac{1}{\beta^{\alpha}\tau(\alpha)}x^{\alpha-1}e^{\frac{-x}{\beta}} \quad (3)$$

where α>0 is a shape parameter, β>0 denotes a scale parameter, and $\tau(\alpha)$ represents the ordinary gamma function of α.

As an extension of the SPI, Vicente-Serrano et al. (2010) proposed the SPEI by including both *P* and potential *ET* (*PET*) in identifying drought. Here, the PET was estimated by the FAO-56 Penman-Monteith (PM) method included in the VIC model (Allen et al., 1998). The SPEI was derived through the following steps: (1) the difference between *P* and *PET* for the *i*th month is calculated as: $D_i = P_i\text{-}PET_i$; (2) the D_i is aggregated at a certain (e.g., 3-month) timescale; and (3) the following log-logistic probability distribution *g(x)* is used to fit the D_i to calculate SPEI:

$$f(x)=\frac{\varphi}{\psi}\left(\frac{x-\gamma}{\psi}\right)^{\varphi-1}\left[1+\left(\frac{x-\gamma}{\psi}\right)^{\varphi}\right]^{-2} \quad (4)$$

where φ, ψ, and γ are the scale, shape and origin parameters, respectively. The *D* is in the range of $\gamma < D < \infty$.

The SPI and SPEI can be used to quantify *P* deficit at multiple timescales (e.g., 1, 3, 6, 12, 24 and 36 months). The short time scale SPI/SPEI (e.g., 1-month) reflects short-term dryness and wetness conditions and are sensitive to *P* short-term changes in general. Whereas, the long timescale SPI/SPEI (e.g., 24-month) reflects the long-term (small) variation of dryness and wetness (WMO, 2016). In this study, the 3-month scale is used to compute the SPI and SPEI (i.e., SPI3 and SPEI3) because it reflects seasonal variation of dryness and wetness conditions. The SPI is calculated based on the *P* from the GCMs outputs, and the SPEI is calculated based on the *P* from GCMs and PET simulated by the VIC model forced by the GCM outputs. The drought classifications based on the SPI and SPEI are shown in Table 2.

3.3.2 PDSI

The PDSI is based on the concept of climatically appropriate for existing conditions (*CAFEC*) proposed by Palmer (1965). It can be used to describe the degree of water deficit in a specific region less than the appropriate moisture content of the local climate. In this study, the *P* from the GCM outputs, and the *PET*, *ET*, *SM* (the top two soil layers) and *RO* simulated by the VIC model forced by the GCM outputs are used to estimate recharge to soils (*R*), water loss to soil layers (*L*), potential recharge (*PR*), potential runoff (*PRO*), and potential loss (*PL*) to derive *CAFEC* at the monthly scale. Then the PDSI is computed based on the difference between *P* and *CAFEC*. The *CAFEC* represents the amount of *P* required to keep a normal *SM* level for a given time, which is defined as:

$$CAFEC = \alpha_i PET + \beta_i PR + \gamma_i PRO - \delta_i PL \quad (5)$$

where *i* indicates the calendar month of a year (from 1 to 12). α_i, β_i, γ_i and δ_i are climatological coefficients expressed as:

$$\alpha_i = \frac{\overline{ET_i}}{\overline{PET_i}} \quad \beta_i = \frac{\overline{R_i}}{\overline{PR_i}} \quad \gamma_i = \frac{\overline{RO_i}}{\overline{PRO_i}} \quad \delta_i = \frac{\overline{L_i}}{\overline{PL_i}} \quad (6)$$

The difference between *P* and *CAFEC* for a particular month is the moisture departure ($d = P - CAFEC$). The climatological standardization process aims to use *d* as a standardized drought index, considering local climate and drought duration, and the self-calibrating procedure (Wells et al., 2004):

$$\begin{cases} Z = K_1 \times K_2 \times d_i \\ X_1 = qZ_1 \\ X_i = pX_{i\text{-}1} + qZ_i \end{cases} \quad (7)$$

where *Z* is the moisture anomaly index for the *i*th month; K_1 denotes the temporal correction weight; K_2 represents the spatial correction weight; *p* and *q* are duration factors; and X_{i-1} is the PDSI for the previous month. For more information on the calculation of K_1, K_2, *p* and *q*, please refer to Wells et al. (2004). Table 2 shows the classification of drought in accordance to the PDSI definition.

3.3.3 Drought area and frequency

Based on the classification definition of drought (Table 2), a threshold value of -1 (-0.5) for PDSI (SPI/SPEI) is used to identify the occurrence of drought. Drought area is defined as:

$$D_a = \frac{\sum_{i=1}^{n} d_a}{n_a} \times 100 \tag{8}$$

where D_a is the percentage of drought area (%), d_a is the number of grid points with PDSI ≤ -1 (SPI/SPEI ≤ -0.5), and n_a is total number of grid points.

$$D_F = \frac{n_m}{N_m} \times 100 \tag{9}$$

where D_F is the drought frequency (%), n_m and N_m are the number of drought months and the total number of months, respectively.

3.4 Variance-based sensitivity analysis framework

In this study, the variance-based two-layer sensitivity analysis framework was used to quantify the uncertainty of GCMs and RCP scenarios in the projection of future drought indices (Dai et al., 2017; Xu et al., 2019b). In this framework, the model with a form of $\Delta = f(\theta) = f(\theta_1, \ldots, \theta_k)$ is a set of uncertain model inputs, with total variance ($V(\Delta)$) being decomposed as:

$$V(\Delta) = V_{\theta_i}(E_{\theta_{\sim i}}(\Delta \mid \theta_i)) + E_{\theta_i}(V_{\theta_{\sim i}}(\Delta \mid \theta_i)) \tag{10}$$

where Δ is the objective function of the model output and $\theta = \{\theta_1, \ldots, \theta_k\}$. $V_{\theta_i}(E_{\theta_{\sim i}}(\Delta \mid \theta_i))$ is the partial variance contributed by θ_i, while $E_{\theta_i}(V_{\theta_{\sim i}}(\Delta \mid \theta_i))$ represents the partial variance caused by model inputs apart from θ_i and interactions amongst all inputs (Dai and Ye, 2015; Dai et al., 2017).

Based on Eq. (10), the total variance ($V(\Delta)$) is decomposed as:

$$\begin{aligned} V(\Delta) &= E_{\mathbf{R}} V_{\mathbf{S|R}}(\Delta \mid \mathbf{R}) + V_{\mathbf{R}} E_{\mathbf{S|R}}(\Delta \mid \mathbf{R}) \\ &= V(\mathbf{S}) + V(\mathbf{R}) \end{aligned} \tag{11}$$

where **R** is the set of multiple RCP scenarios, and **S** is the set of multiple GCMs. The subscript $\mathbf{S}|\mathbf{R}$ indicates the change of GCMs under particular RCP scenario. The terms in Eq. (11) refer to variances from RCP scenarios and GCMs uncertainty, respectively. The sensitivity of RCPs ($S_{\boldsymbol{R}}$) and GCMs ($S_{\boldsymbol{S}}$) can then be determined as follows:

$$
\begin{aligned}
S_R &= \frac{V_{\mathbf{R}} E_{\mathbf{S|R}}(\Delta \mid \mathbf{S},\mathbf{R})}{V(\Delta)} = \frac{V(\mathbf{R})}{V(\Delta)} \\
S_S &= \frac{E_{\mathbf{R}} V_{\mathbf{S|R}}(\Delta \mid \mathbf{S},\mathbf{R})}{V(\Delta)} = \frac{V(\mathbf{S})}{V(\Delta)}
\end{aligned}
\tag{12}
$$

For each drought index (PDSI, SPI3 and SPEI3), the mean and variance of outputs with respects to uncertainty from GCMs under certain RCP scenario are calculated, and the mean and variance of RCP scenarios are quantified. Assume that there are k alternative RCP scenarios and n plausible GCMs for each RCP scenario, the uncertainty of GCMs is estimated as:

$$
\begin{aligned}
V(\mathbf{S}) &= E_{\mathbf{R}} V_{\mathbf{S|R}}(\Delta \mid \mathbf{S},\mathbf{R}) \\
&= \sum_k \left(\frac{1}{n}\sum_{i=1}^{n} \Delta^2\left(S_i \mid R_k\right) - \left(\frac{1}{n}\sum_{i=1}^{n} \Delta\left(S_i \mid R_k\right) \right)^2 \right) P\left(R_k\right)
\end{aligned}
\tag{13}
$$

where $P\left(R_k\right)$ is the weight of RCP scenario, subject to $\sum_k P\left(R_k\right) = 1$, and the uncertainty of RCP scenarios is deduced as:

$$
\begin{aligned}
V(\mathbf{R}) &= V_{\mathbf{R}} E_{\mathbf{S|R}}(\Delta \mid \mathbf{R}) \\
&= E_{\mathbf{R}}\left(E_{\mathbf{S|R}}\left(\Delta \mid \mathbf{R}\right)\right)^2 - \left(E_{\mathbf{R}} E_{\mathbf{S|R}}\left(\Delta \mid \mathbf{R}\right)\right)^2 \\
&= \sum_k P\left(R_k\right)\left(\frac{1}{n}\sum_{i=1}^{n} \Delta\left(S_i \mid R_k\right) \right)^2 - \left(\sum_k \left(\frac{1}{n}\sum_{i=1}^{n} \Delta\left(S_i \mid R_k\right) \right) P\left(R_k\right) \right)^2
\end{aligned}
\tag{14}
$$

4. Results

4.1 Evaluation of GCM and VIC simulations

Fig. 2 shows the comparison between the observed and bias-corrected monthly average T and P of 30 simulation samples of 13-GCM ensembles in the West River (Fig. 2a, 2c) and North River (Fig. 2b, 2d) basins for the baseline period 1971-2000. As shown in Fig. 2, the majority of model simulations reproduce the intra-annual variability of T reasonably well (despite a bit underestimation in a few months).

Compared with T, greater uncertainty range is identified in the simulations of P, especially in the flood season (May-August). Moreover, larger uncertainty range is found in the North River basin compared to the West River basin. Overall, the bias-corrected model simulations can simulate the intra-annual variability of P for the two basins, particularly for the dry season (October-March).

Fig. 3 demonstrates the comparison of simulated and observed daily discharges at the Gaoyao and Hengshi stations for the calibration and validation periods. The daily Nash-Sutcliffe efficiency coefficient (NSE) at the Gaoyao and Hengshi stations are 0.85 and 0.9 (0.89 and 0.9) in the calibration (validation) period, respectively, and the relative errors (Res) are 7.25% and 2.95% (0.21% and 0.42%), respectively, in the calibration (validation) period. Overall, the VIC model can reproduce the low discharge accurately during dry season and the flood peak during flooding season, and the occurrence time is generally consistent between the observed and simulated ones, indicating that the VIC model is applicable for subsequent GCM-projections of drought.

Fig. 4 shows the comparison of the simulated PDSI, SPI3 and SPEI3 with the observed ones in the West and North River basins during the baseline period 1971-2000. As witnessed in Fig. 4, the model simulations tend to underestimate the variability of PDSI, SPI3 and SPEI3, and fail to capture some extreme wet and dry events in wet and dry years, particularly in the West River basin. Compared with PDSI, the temporal variability of SPI and SPEI tends to be large for both basins, bringing challenges for the model to simulate the dryness/wetness conditions characterized by SPI and SPEI. Overall, the three drought indices are simulated more accurately in the North River basin than West River basin.

4.2 Sensitivity of projected D_a changes to index definition, GCM ensemble and RCP

This section focuses on the sensitivity analysis of projected drought area changes to index definition, GCM ensemble and RCP scenario. Fig. 5 reveals the temporal evolutions (2021-2050) of the projected changes in D_a indicated by the PDSI ($\leq$ -1), SPI3 ($\leq$ -0.5) and SPEI3 ($\leq$ -0.5) for the future period 2021-2050 (relative to the baseline period) in the two basins under three RCP scenarios. Clearly, there are obvious differences in projected D_a changes between different indices. However, compared with PDSI, SPI and SPEI demonstrate more similar and larger temporal variability of the projected D_a changes for both basins. Large GCM spread (uncertainty range) is found in projected D_a changes, especially in the North River basin, which is significantly larger than that of drought indices and RCPs. In contrast, there are relatively small differences in projected D_a changes under three RCP scenarios compared with GCMs and drought indices.

4.3 Sensitivity of projected D_F changes to index definition, GCM ensemble and RCP

This section focuses on the sensitivity analysis of the projected D_F to index definition, GCM ensemble and RCP scenario. The projected D_F changes indicated by the PDSI, SPI3 and SPEI3 with extreme, severe, moderate and mild drought events for the West and North River basins during the future period 2021-2050 under three RCP scenarios were calculated (relative to the baseline period 1971-2000).

Fig.6 shows the uncertainty range (GCM spread) of the projected D_F changes (%) indicated by three drought indices under three RCP scenarios. From the figure, clearly there is a large GCM spread in the projected D_F changes (especially for that indicated by SPEI) under all RCP scenarios, with the larger GCM spread in the North River basin than West River basin. In contrast, the RCP discrepancy in the projected D_F changes is generally smaller compared with GCM. In terms of drought events, larger GCM uncertainty range is found for the projected changes in extreme drought than other drought events. There are also large discrepancies in the sign and magnitude of the projected D_F changes amongst three drought indices (especially between SPI and PDSI/SPEI). The SPI tends to underestimate the projected changes in D_F compared with PDSI and SPEI in the West River basin.

Fig.6a also reveals the increased D_F indicated by the PDSI (SPEI3) is projected for all drought events (extreme, severe, moderate and mild) in the West River basin, especially for extreme drought, with the mean increases up to 15% (13.7%), 13% (12.3%) and 13.3% (13%) under RCP2.6, RCP4.5 and RCP8.5, respectively. In comparison, the SPI3 detects an increase in extreme drought, with average increase of 10.4%, 10% and 9.1% under RCP2.6, RCP4.5 and RCP8.5, respectively, and a decrease in severe (moderate) drought, with average decrease of -5.3% (-12%), -5.3% (-12%) and -4.9% (-11.6%) under RCP2.6, RCP4.5 and RCP8.5, respectively.

For the North River basin (Fig.6b), the D_F of extreme and mild droughts indicated by three drought indices (PDSI, SPI3 and SPEI3) shows an overall increase under three RCP scenarios. Particularly, SPI3 detects large mean increase in extreme drought (up to 10.1%, and 9.1% and 11.7% under RCP2.6, RCP4.5 and RCP8.5, respectively), whereas SPEI3 detects large mean increase in mild drought (up to 18.3%, and 18.6% and 17.9% under RCP2.6, RCP4.5 and RCP8.5, respectively). In contrast, the D_F of severe drought indicated by three indices is projected to decrease under all 3 RCP scenarios, and SPEI3 shows large mean decrease compared with other indices (up to -11.4%, -12.3% and -10.7% under RCP2.6, RCP4.5 and RCP8.5, respectively). For moderate drought, the projected increases in D_F are indicted by PDSI (SPEI3), with mean increase of 8.4% (1.6%), 8.7% (2.0%) and 8.3% (1.5%) under RCP2.6, RCP4.5 and RCP8.5, respectively.

4.4 Spatial distributions of the projected D_F changes

The spatial distribution of the multi-GCM ensemble mean changes in D_F (indicated by the PDSI, SPI3 and SPEI3) with extreme, severe, moderate and mild drought events for the future period 2021-2050 (relative to the baseline period 1971-2000) under three RCP scenarios are displayed in Figs. 7 and 8 for the West River and North River basins, respectively. Figs. 7 and 8 highlight the sign and magnitude of D_F changes, which are dependent on the index definition, particularly for the North River basin. For a certain drought index, there are significant spatial variation in model projection for both basins.

For the West River basin (Figs.7a~c), there are large spatial difference in the projected D_F changes between SPI and PDSI (SPEI), while similar spatial pattern can be found between PDSI and SPEI3. The projected D_F changes in extreme drought indicated by the PDSI and SPEI3 tend to be more significant than other drought events. The largest D_F changes in extreme drought indicated by the PDSI (15.9%) and SPEI3 (16.4%) are concentrated in the downstream reaches of the West basin, while the decreases are projected mainly in the upstream areas (up to -23.7% and -15.7%, respectively). For SPI3, the projected D_F changes are unevenly distributed in the West River basin, with the largest increase of 9.5% in extreme D_F under RCP8.5 (Fig. 7b). In contrast, the D_F of moderate and mild droughts is projected to decrease in the majority of the West River basin, particularly under RCP4.5 and RCP8.5 (up to -16.7%).

For the North River basin (Figs.8a~c), the projected D_F changes indicated by three drought indices are unevenly distributed at the spatial scale. For PDSI, the D_F of moderate and mild droughts shows larger increase compared with other drought events in major North River basin under three RCP scenarios (Fig. 8a). The D_F of mild drought is increased by 11.3% under RCP2.6, while that of extreme and severe droughts is decreased, especially for severe drought (up to -7.8%). For SPI3, the D_F of extreme drought is projected to increase in the majority of the North River basin under RCP2.6 and RCP4.5 (up to 8.2%), and decrease in the northern parts of the North River basin under RCP8.5 (up to -8.2%). For SPEI3, the projected D_F changes are spatially heterogeneous in the North River basin, with the largest increase of 11.8% in D_F of extreme drought under RCP8.5 (Fig. 8c). In contrast, the D_F of severe drought is projected to decrease in most of the North River basin, especially in the northern regions under RCP2.6 and RCP4.5 (up to -16%).

4.5 Sensitivity indices for the uncertainty contributions to the drought indices projections

The sensitivity indices for the uncertainty contribution of GCM and RCP to the projection of three drought indices (PDSI, SPI and SPEI) were calculated at both spatial (basin) and temporal (interannual) scales using the variance-based sensitivity analysis approach. Fig.9 shows the temporal evolution (2021-2050) of uncertainty contribution (i.e., sensitivity indices) of GCM and RCP to three drought indices (PDSI, SPI and SPEI) projections during the period 2021-2050. From the Figure, GCM plays a dominant role (> 90%) in the projection uncertainty of three drought indices over the entire period for both basins, whereas the uncertainty of RCP is relatively limited compared with GCM. The GCM (RCP) uncertainty tends to be larger (smaller) in the West River basin than the North River basin, while the interannual variability of GCM (RCP) uncertainty is larger in the North River basin than in the West River basin. Overall, the GCM (RCP) uncertainty presents similar pattern amongst three drought indices, but tends to be smaller (larger) in SPI3 than PDSI and SPEI3 projections for both basins.

Fig.10 demonstrates the spatial distribution of GCMs' uncertainty contribution to the projection of PDSI, SPI3 and SPEI3 in the two basins during future three decades (i.e., 2030, 2040 and 2050). As shown in Fig.10, GCM is the leading uncertainty source (> 90%) for the projection of three drought indices for both basins. The uncertainty of GCM is unevenly distributed but with similar spatial patterns among three drought indices in the West River basin (Fig.10a). In addition, the uncertainty of GCM tends to increase (decrease) in the eastern (southwest) regions from 2030 to 2050, while in the southern regions it decreases first and then increases. For the North River basin (Fig.10b), the uncertainty of GCM is unevenly distributed and shows large spatial discrepancies among three drought indices. Overall, the uncertainty of GCM (particularly for the projection of PDSI and SPEI3) tends to decrease in the majority of the North River basin from 2030 to 2050, especially in northeast and southern regions (Fig. 10b).

Fig.11 reveals the overall uncertainty contributions of GCM and RCP to the projection of three drought indices (PDSI, SPI3, and SPEI3) for the two basins. Overall, GCM contributes more than 96% of total uncertainty to the PDSI projection for both basins, while for the projection of SPI3 and SPEI3, the uncertainty contribution of GCM takes over 95% for both basins. Compared with GCM, the uncertainty of RCP is rather limited and can be omitted in the future period (2021-2050) for both basins.

5. Discussion

In this research, we present an assessment of projection and uncertainty of D_F and D_a in the Pearl River basin during the period 2021-2050 based on downscaling simulations (a total of 90 samples) of 13 CMIP5 GCMs under three RCP scenarios. Three different drought indices (i.e., PDSI, SPI3 and SPEI3) are employed to explore the spatio-temporal changes in D_F and D_a with different (extreme, severe, moderate and mild) drought events. The uncertainty in the projection of three drought indices derived from GCMs and RCPs is quantified using variance-based sensitivity analysis approach.

The results show that the sign and magnitude of the projected changes in drought characteristics (e.g., D_F and D_a) are highly dependent on the index definition at both spatial and temporal scales, generally consistent with the findings from previous studies (e.g., Burke and Brown, 2008; Mishra and Singh, 2010; Touma et al., 2015; Lee et al., 2019; Yang et al., 2019). This suggests that any single index may suffer from limitations in considering the different aspects of droughts comprehensively. In particular, the SPI tends to underestimate the projected changes in D_F in both basins compared with PDSI and SPEI, which might be due to that the SPI considers *P* deficit alone without taking into account the impact of *ET* in the context of climate warming (Jeong et al., 2014; Rhee and Cho, 2016; Yoo et al., 2016; Ahmadalipour et al., 2017; Huang et al., 2018; Lee et al., 2019; Haile et al., 2020; Wu et al., 2020).

The results also highlight a large discrepancy in the projected D_F and D_a changes amongst different GCM ensembles (Figs. 4-6), and larger model spread is found in the projected D_F and D_a changes of extreme drought than other drought events (Fig.6). This is in consistency with previous studies showing a large uncertainty among GCMs when projecting drought events in 21st century using CMIP3 and CMIP5 ensemble (Sheffield and Wood, 2008; Dai, 2013; Orlowsky and Seneviratne, 2013). The uncertainty analysis suggests that the GCM uncertainty, as expected, plays an important role (contribution > 90%) in the projections of drought indices in both basins, while the uncertainty of RCP is generally limited compared with GCM (Figs. 9 and 11). This is supported by Figs. 5 and 6, showing that there are larger discrepancies in projected D_a and D_F among GCM ensembles than RCPs. Such finding is also generally consistent with the previous studies on the projection of meteorological droughts (Wu et al., 2021), extreme temperatures (Wilby and Harris 2006; Woldemeskel et al., 2016; Xu et al., 2019c), precipitation (Zhou et al, 2014; Woldemeskel et al., 2016; Hosseinzadehtalaei et al, 2017; Zarekarizi et al., 2018;Xu et al., 2019b; Kim et al., 2020), and floods (Graham et al., 2007; Kay et al., 2009; Jung et al., 2011; Addor et al, 2014; Giuntoli et al., 2015; Vetter et al., 2017). All these literatures indicated that the uncertainty caused by GCM is larger than that of RCP.

This study also highlights a large spatio-temporal variability of uncertainty in the regional projection of drought characteristics. At the spatial scale, the uncertainty of GCM is unevenly distributed and show similar spatial patterns amongst three drought indices in the West River basin, while in the North River basin the uncertainty of GCM shows large spatial discrepancies amongst three drought indices (Fig.10). At the interannual scale, the uncertainty of GCM shows a large variability, and the variability tends to be larger in the North River basin than in the West River basin (Fig.9). This is generally consistent with the previous studies (Xu et al., 2019b; Wu et al., 2021), which indicated that the uncertainty of GCM and RCP in drought prediction has large temporal and spatial variations at the regional scale. Spatially, GCM has relatively larger uncertainty in the Southern Hemisphere than the Northern Hemisphere, whereas RCP has relatively larger uncertainty in the Northern Hemisphere than the Southern Hemisphere (Wu et al., 2021). At the temporal scale, the GCM uncertainty shows overall decreasing trends with time (Xu et al., 2019b; Wu et al., 2021). In contrast, the RCP uncertainty is expected to increase over time until the end of this century, but remains less than that of GCM at the regional (Xu et al., 2019b) and global (Wu et al., 2021) scales. The spatio-temporal variability of the uncertainties in GCM-based drought projection, might be due to the results of disagreement on the magnitude of warming, as well as the magnitude and sign of P changes at the regional scale (Trenberth et al., 2014).

Within this study, we did not consider some other potential sources of uncertainty that arise not only from the methods but also from the simulations themselves. First, although the bias-corrected method shows significant improvement in the simulations of T and P, there are still relatively large errors (especially for P) in few months (see Fig. 2), which may lead to potential uncertainty. Particularly, the GCM simulations fail to capture some extreme events in wet/dry years, particularly in the West River basin (Fig. 4). This means that the bias-corrected method may reduce the variability range of the GCM simulations, leading to an underestimation of GCM uncertainty in the projections of drought indices (SPI, PDSI, SPEI) during extreme wet and dry years. This is supported by Wu et al. (2021), which indicated that the bias-corrected method can be an important uncertainty source in explaining the model difference in the projection of meteorological droughts. Second, the definitions of D_F and D_a are based only on the threshold of (-1 for PDSI and -0.5 for SPI and SPEI) of drought indices, without quantifying the drought events statistically. The choice of methods to define drought characteristics can also lead to model discrepancies in drought projection (Mo, 2008; Sheffield and Wood, 2008; Dai, 2011b). In addition, we only consider one hydrological model (VIC) in the hydrological simulations. Hydrological models themselves may be biased due to inadequacies in the modeled physical processes and parameterizations and because of processes that are not include in the modeling, the structure of hydrological model can be an important source of uncertainty in climate change assessment (Graham et al., 2007; Kay et al., 2009; Addor et al, 2014; Eisner et al., 2017; Su et al., 2017; Vetter et al., 2017; Ju et al., 2021). The PDSI and SPEI were partly calculated based on hydrological simulations. This means that the uncertainty of hydrological model is included in the uncertainty of GCM and RCP, which may lead to the overestimation of the uncertainty of GCM and RCP in the projections of PDSI and SPEI. In future research, it would be interesting to explore more sources of uncertainty (e.g., hydrological model, bias-corrected method, and the definition of drought) with the consideration of multiple-model ensembles, which are essential for assessing drought projection reliably in response to climate warming at both regional and basin scales.

6. Conclusions

This research assesses the projection and uncertainty of drought characteristics (D_F and Da) in the Pearl River basin during the period 2021-2050 using three different drought indices (PDSI, SPI and SPEI) based on 13 CMIP5 GCMs under three RCP scenarios. The SPI is calculated based on the P simulations of 13 GCMs, while the PDSI and SPEI are computed based on the simulations of the VIC model forced by 13 GCMs. The uncertainty of projected drought indices (PDSI, SPI and SPEI) due to various GCMs and RCPs is quantified by the variance-based sensitivity analysis approach.

The results show that there are large discrepancies in the sign and magnitude of D_F and Da changes amongst three drought indices, and the SPI tends to underestimate the projected changes in D_F in both basins compared with PDSI and SPEI. In terms of a particular drought index, there are significant spatial variation in the model projection of D_F. There is also a large model spread in the projected D_F and D_a changes among different GCM ensembles, and larger model spread is found in the projected extreme drought than other drought events. Overall, the D_F of extreme drought is projected to increase in the future period (2021-2050) in both basins, especially for the North River basin.

The uncertainty analysis results show that GCM is the dominant uncertainty (contribution > 90%) in the projections of three drought indices, while the uncertainty of RCP is relatively limited compared with GCM. The uncertainty of GCM and RCP shows a large interannual variability during the future period, with larger variability in the North River basin than Wet River basin. At the spatial scale, the uncertainty of GCM is unevenly distributed and show similar spatial patterns among three drought indices in the West River basin, while the uncertainty of GCM in the North River basin shows large spatial discrepancies amongst three drought indices. By the end of 2050, the uncertainty of GCM tends to increase in the Eastern regions of the Wet River basin and decrease in the Northeast and Southern regions of the North River basin. This study highlights the sensitivity of drought projection to the index definition as well as the large spatial-temporal variability of general uncertainty sources in drought projections.

Acknowledgements

This research was supported by funding from the 2019 International Program of Guangdong Provincial Outstanding Yong Researcher, the China Postdoctoral Science Foundation (Grant No. 2020M673073), the National Natural Science Foundation of China (Grant No. 51909106, 51879108, 51709127), the Natural Science Foundation of Guangdong Province, China (Grant No. 2020A1515011038, 2018A030310653), the high-level talent project for the “Pearl River Talent Plan” of Guangdong Province (Grant No. 2017GC010397), and the Youth Innovative Talents Project for Guangdong

Colleges and Universities (Grant No. 2017KQNCX010).

References

Addor N., Rössler O., Köplin K., Huss M., Weingartner R., Seibert J., 2014. Robust changes and sources of uncertainty in the projected hydrological regimes of Swiss catchments. *Water Resour. Res.*, 50, 7541–7562. https://doi.org/10.1002/2014WR015549.

Ahmadalipour A., Moradkhani H., Demirel M.C., 2017. A comparative assessment of projected meteorological and hydrological droughts: Elucidating the role of temperature. *J. Hydrol.*, 553, 785–797. https://doi.org/10.1016/j.jhydrol.2017.08.047.

Allen R.G., Pereira L.S., Raes D. & Smith M., 1998. Crop Evapotranspiration-Guidelines for computing crop water requirements. Food and Agricultural Organization of the United Nations Irrigation and Drainage Paper, 56 300 (8): D05109.

American Meteorological Society (AMS), 2004. Statement on Meteorological Drought. *Bull. Am. Meteorol. Soc.*, 85, 771–773. https://www.ametsoc.org/POLICY/2013drought_amsstatement.html.

Amnuaylojaroen T., Chanvichit P., 2019. Projection of near-future climate change and agricultural drought in Mainland Southeast Asia under RCP8.5. *Clim. Chang.*, 155(2), 175–193. https://doi.org/10.1007/s10584-019-02442-5.

Burke E.J., Brown S.J., 2008. Evaluating uncertainties in the projection of future drought. *J. Hydrometeorol.*, 9(2), 292–299. https://doi.org/10.1175/2007JHM929.1.

Cook B.I., Smerdon J.E., Seager R., Coats S., 2014. Global warming and 21st century drying. *Clim. Dyn.*, 43(9-10), 2607–2627. https://doi.org/10.1007/s00382-014-2075-y.

Chen J., Brissette F.P. & Leconte R., 2011. Uncertainty of downscaling method in quantifying the impact of climate change on hydrology. *J. Hydrol.*, 401(3-4), 190–202. https://doi.org/10.1016/j.jhydrol.2011.02.020.

Chen L., Frauenfeld O.W., 2014. Surface air temperature changes over the twentieth and twenty-First centuries in China simulated by 20 CMIP5 models. *J. Clim.*, 27 (11), 3920–3937. https://doi.org/10.1175/JCLI-D-13-00465.1.

Chen Y.D., Zhang Q., Xiao M., Singh V.P., 2017. Transition probability behaviors of drought events in the Pearl River basin, China. *Stoch. Environ. Res. Risk Assess.*, 31(1), 159–170. https://doi.org/10.1007/s00477-015-1178-2.

Dai A.G., 2011a. Characteristics and trends in various forms of the Palmer Drought Severity Index during 1900-2008. *J. Geophys. Res.*, 116(D12), 1248–1256. https://doi.org/10.1029/2010JD015541.

Dai A.G., 2011b. Drought under global warming: A review. *Wiley Interdiscip. Rev.: Clim. Change*, 3, 52–58. https://doi.org/10.1002/wcc.81; Corrigendum, 3, 167, https://doi.org/10.1002/wcc.190.

Dai A.G., 2013. Increasing drought under global warming in observations and models. *Nat. Clim. Change.*, 3(2), 52–58. https://doi.org/10.1038/NCLIMATE1633.

Dai H., Ye M., 2015. Variance-based global sensitivity analysis for multiple scenarios and models with implementation using sparse grid collocation. *J. Hydrol.*, 528, 286–300. https://doi.org/10.1016/j.jhydrol.2015.06034.

Dai H., Ye M., Walker A.P., Chen X.Y., 2017. A new process sensitivity index to identify important system processes under process model and parametric uncertainty. *Water Resour. Res*., 53, 3476–3490. https://doi.org/10.1002/2016WR019715.

Eisner S., Flörke M., Chamorro A., et al. 2017. An ensemble analysis of climate change impacts on streamflow seasonality across 11 large river basins. *Clim. Change*, 141(3), 401–417. https://doi.org/10.1007/s10584-016-1844-5.

FAO, IIASA, ISRIC, ISSCAS, 2009. Harmonized World Soil Database Version 1.1.

Fischer T., Gemmer M., Liu L.L., Su B.D., 2011. Temperature and precipitation trends and dryness/wetness pattern in the Zhujiang River Basin, South China, 1961-2007. *Quatern. Int*., 244(2), 138–148. https://doi.org/ 10.1016/j.quaint.2010.08.010.

Fischer T., Gemmer M., Su B., Scholten T., 2013. Hydrological long-term dry and wet periods in the Xijiang River basin, South China. *Hydrol. Earth Syst. Sci*., 17 (1), 135–148. https://doi.org/10.5194/hess-17-135-2013.

Fowler H.J., Blenkinsop S., Tebaldi C., 2007. Linking climate change modelling to impacts studies: recent advances in downscaling techniques for hydrological modelling. *Int. J. Climatol*., 27, 1547–1578. https://doi.org/10.1002/joc.1556.

Giuntoli I., Vidal J.P., Prudhomme C., and Hannah D.M., 2015. Future hydrological extremes: the uncertainty from multiple global climate and global hydrological models. *Earth Syst. Dynam*., 6, 267–285. https://doi.org/10.5194/esd-6-267-2015.

Graham L.P., Hagemann S., Jaun S. and Beniston M., 2007. On Interpreting Hydrological Change From Regional Climate Models. *Clim. Change*, 81, 97–122. https://doi.org/10.1007/s10584-006-9217-0.

Gudmundsson L., Seneviratne S.I., and Zhang X., 2017. Anthropogenic climate change detected in European renewable freshwater resources. *Nat. Clim. Change*, 7(11), 813–816. https://doi.org/10.1038/nclimate3416.

Haile G.G., Tang Q., Hosseini-Moghari S.-M., Liu X., Gebremicael T.G., Leng G., Kebede A., Xu X., and Yun X., 2020. Projected impacts of climate change on drought patterns over East Africa. *Earth's Future*, 8(7), e2020EF001502. https://doi.org/10.1029/2020EF001502.

Hansen M.C., Defries R.S., Townshend R.G., and Sohlberg R., 2000. Global land cover classification at 1 km spatial resolution using a classification tree approach. *Int. J. Remote Sens*., 21, 1331–1364. https://doi.org/10.1080/014311600210209.

Hay L.E., Wilby R.L. and Leavesley G.H., 2000. A comparison of delta change and downscaled GCM scenarios for three mountainous basins in the United States. *J. Am. Water Resour. Assoc*., 36(2), 387–397. https://doi.org/10.1111/j.1752-1688.2000.tb04276.x.

Hayes M.J., Svoboda M.D., Wilhite D.A., Vanyarkho, O.V., 1999. Monitoring the 1996 drought using the standardized precipitation index. *Bull. Am. Meteorol. Soc*., 80(3), 429–438. https://doi.org/10.1175/1520-0477(1999)080<0429:MTDUTS>2.0.CO;2.

Hayes M, Svoboda M, Wall N, and Widhalm M, 2011. The Lincoln Declaration on Drought Indices: Universal Meteorological Drought Index Recommended. *Bull. Am. Meteorol. Soc*., 92(4), 485–488. https://doi.org/10.1175/2010BAMS3103.1.

Heim R.R Jr., 2002. A review of twentieth-century drought indices used in the United States. *Bull. Am. Meteorol. Soc*., 83(8), 1149–1165. https://doi.org/10.1175/1520-0477-83.8.1149.

Huang D.Q., Zhu J., Zhang Y.C., Huang A.N., 2013. Uncertainties on the simulated summer precipitation over Eastern China from the CMIP5 models. *J. Geophys. Res. Atmos*., 118 (16), 9035–9047. https://doi.org/10.1002/jgrd.50695.

Huang S.Z., Chang J.X., Huang, Q., Chen, Y.T., 2014. Spatio-temporal Changes and Frequency Analysis of Drought in the Wei River Basin, China. *Water Resour. Manag.*, 28(10), 3095–3110. https://doi.org/10.1007/s11269-014-0657-4.

Huang J., Ji M., Xie Y., Wang S., He Y., and Ran J., 2016. Global semi-arid climate change over last 60 years. *Climate Dyn.*, 46, 1131–1150. https://doi.org/10.1007/s00382-015-2636-8.

Huang J.L., Zhai J.Q., Jiang T., Wang Y.J., Li X.C., Wang R., Xiong M., Su B.D., Fischer T., 2018. Analysis of future drought characteristics in China using the regional climate model CCLM. *Clim. Dyn.*, 50(1-2), 507–525. https://doi.org/10.1007/s00382-017-3623-z.

Hollinger S.E., Isard S.A., Welford M.R., 1993. A new soil moisture drought index for predicting crop yields. In: Preprints, Eighth Conf. on Applied Climatology, Anaheim, CA, Am Meteor Soc, pp. 187–190.

Hosseinzadehtalaei P., Tabari H. & Willems P., 2017. Uncertainty assessment for climate change impact on intense precipitation: How many model runs do we need? *Int. J. Climatol.*, 37, 1105–1117. https://doi.org/10.1002/joc.5069.

IPCC. Climate Change 2007: The physical science basis[M]. Cambridge: Cambridge University Press, 2007.

IPCC (2013) Climate Change 2013: The Physical Science Basis. Contribution of Working Group I to the Fifth Assessment Report of the Intergovernmental Panel on Climate Change [Stocker TF, Qin D, Plattner G-K, Tignor M, Allen SK, Boschung J, Nauels A, Xia Y, Bex V, Midgley PM (eds)]. Cambridge University Press: Cambridge, United Kingdom and New York, NY, USA, pp 1535. https://doi.org/10.1017/CBO9781107415324.

Jeong D.I., Sushama L. & Naveed Khaliq M., 2014. The role of temperature in drought projections over North America. *Clim. Change*, 127, 289–303. https://doi.org/10.1007/s10584-014-1248-3.

Ju J.L., Dai H., Wu C.H., Hu B.X., Ye M., Chen X.Y., Gui D.W., Liu H.F. and Zhang J., 2021. Quantifying the Uncertainty of the Future Hydrological Impacts of Climate Change: Comparative Analysis of an Advanced Hierarchical Sensitivity in Humid and Semiarid Basins. *J. Hydrometeor.*, DOI: https://doi.org/10.1175/JHM-D-20-0016.1.

Jung I.W., Chang H.J., and Moradkhani H., 2011. Quantifying uncertainty in urban flooding analysis considering hydro-climatic projection and urban development effects. *Hydrol. Earth Syst. Sci.*, 15, 617–633. https://doi.org/10.5194/hess-15-617-2011.

Kay A.L., Davies H.N., Bell V.A., Jones R.G., 2009. Comparison of uncertainty sources for climate change impacts: flood frequency in England. *Clim. Change*, 92(1-2), 41–63. https://doi.org/10.1007/s10584-008-9471-4.

Keyantash J., and Dracup J. A., 2002. The quantification of drought: An evaluation of drought indices. *Bull. Amer. Meteor. Soc.*, 83(8), 1167–1180. https://doi.org/10.1175/1520-0477-83.8.1167.

Kharin V.V., Zwiers F.W., Zhang X., Wehner M., 2013. Changes in temperature and precipitation extremes in the CMIP5 ensemble. *Clim. Change*, 119, 345–357. https://doi.org/10.1007/s10584-013-0705-8.

Kim S., Eghdamirad S., Sharma A. & Kim, J.H., 2020. Quantification of uncertainty in projections of extreme daily precipitation. Earth and Space Science, 7(8), e2019EA001052. https://doi.org/10.1029/2019EA001052.

Lafon T., Dadson S., Buys G. and Prudhomme C., 2013. Bias correction of daily precipitation simulated by a regional climate model: a comparison of methods. *Int. J. Climatol.*, 33, 1367–1381. https://doi.org/10.1002/joc.3518.

Lee M.H., Im E.S., Bae D.H., 2019. A comparative assessment of climate change impacts on drought over Korea based on multiple climate projections and multiple drought indices. *Clim. Dyn.*, 53, 389–404. https://doi.org/10.1007/s00382-018-4588-2.

Li Z., Zheng F., Liu W., 2012. Spatiotemporal characteristics of reference evapotranspiration during 1961-2009 and its projected changes during 2011-2099 on the Loss Plateau of China. *Agric. For. Meteorol.*, 154-155, 147–155. https://doi.org/10.1016/j.agrformet.2011.10.019.

Liang X., Lettenmaier D.P., Wood E.F., and Burges S.J., 1994. A simple hydrologically based model of land surface water and energy fluxes for general circulation models. *J. Geophy. Res.*, 99(D7), 14415–14428. https://doi.org/10.1029/94JD00483.

Liang X., Lettenmaier D.P., Wood E.F., 1996. Surface soil moisture parameterization of the VIC-2L model: Evaluation and modification. *Glob. Planet. Chang.*, 13(1-4): 195–206. https://doi.org/ 10.1016/0921-8181(95)00046-1.

Mckee T.B., Doesken N.J., Kleist J. The relationship of drought frequency and duration to time scales. In: Eighth conference on applied climatology, American meteorological society, Anaheim, CA;1993.

Mishra A.K., Desai V.R., 2005. Drought forecasting using stochastic models. *Stoch. Env. Res. Risk A.* 19(5), 326–339. https://doi.org/10.1007/s00477-005-0238-4.

Mishra A.K., Singh V.P., 2010. A review of drought concepts. *J. Hydrol.*, 391(1-2), 202–216. https://doi.org/10.1016/j.jhydrol.2010.07.012.

Mishra A.K., Singh V.P., 2011. Drought modeling–A review. *J. Hydrol.*, 403(1-2), 157–175. https://doi.org/10.1016/j.jhydrol.2011.03.049.

Mo K.C., 2008. Model-Based Drought Indices over the United States. *J. Hydrometeor.*, 9(6), 1212–1230. https://doi.org/10.1175/2008JHM1002.1.

Moss R.H. and Coauthors, 2010. The next generation of scenarios for climate change research and assessment. *Nature*, 463, 747–756. https://doi.org/10.1038/nature08823.

Nakićenović N. and Coauthors, 2000. *Special Report on Emissions Scenarios* (SRES): A Special Report of Working Group III of the Intergovernmental Panel on Climate Change. N. Nakićenović and R. Swart, Eds., Cambridge University Press, 570 pp.

Niu J., Chen J., Sun L., 2015. Exploration of drought evolution using numerical simulations over the Xijiang (West River) basin in South China. *J. Hydrol.*, 526, 68–77. https://doi.org/10.1016/j.jhydrol.2014.11.029.

Orlowsky B., Seneviratne SI., 2013. Elusive drought: uncertainty in observed trends and short- and long-term CMIP5 projections. *Hydrol. Earth Syst. Sci.* 17(5), 1765–1781. https://doi.org/10.5194/hess-17-1765-2013.

Palmer W. Meteorological drought, Weather Bur. Res. Rap. 45. US Department of Agriculture, US Gov. Print. Off., Washington, DC, 1965.

Palmer W.C., 1968. Keeping track of crop moisture conditions, nationwide: the new crop moisture index. *Weatherwise*, 21(4), 156–161.https://doi.org/10.1080/00431672.1968.9932814.

Peters G, Bier G, van Lanen H.A.J., Torfs P.J.J.F., 2006. Propagation and spatial distribution of drought in a groundwater catchment. *J. Hydrol.*, 321(1-4), 257–275. https://doi.org/10.1016/j.jhydrol.2005.08.004.

Piao S.L., Ciais P., Huang Y., Shen Z.H., Li S.J., Zhou L.P. et al., 2010. The impacts of climate change on water resources and agriculture in China. *Nature*, 467(7311), 43–51, https://doi.10.1038/nature09364.

Rhee J.Y., and Cho J., 2016. Future Changes in Drought Characteristics: Regional Analysis for South Korea under CMIP5 projections. *J. Hydrometeorol*., 17, 437–451. https://doi.org/10.1175/JHM-D-15-0027.1.

Rudd A.C., Kay A.L., Bell V.A., 2019. National-scale analysis of future river flow and soil moisture droughts: potential changes in drought characteristics. *Clim*. *Change*, 156(3), 323–340. https://doi.org/10.1007/s10584-019-02528-0.

Ruosteenoja K., Markkanen T., Venalainen A., Raisanen P., Peltola H., 2018. Seasonal soil moisture and drought occurrence in Europe in CMIP5 projections for the 21st century. *Clim*. *Dyn*., 50(3-4), 1177–1192. https://doi.org/10.1007/s00382-017-3671-4.

Samaniego L., Thober S., Kumar R., Wanders N., Rakovec O., Pan M., Zink M., Sheffield J., Wood E., and Marx A., 2018. Anthropogenic warming exacerbates European soil moisture droughts. *Nat*. *Clim*. *Change*, 8(5), 421–426. https://doi.org/10.1038/s41558-018-0138-5.

Saxton, K.E., Rawls, W.J., 2006. Soil water characteristic estimates by texture and organic matter for hydrologic solutions. *Soil Sci. Soc. Am. J*., 70 (5), 1569–1578. https://doi.org/10.2136/sssaj2005.0117.

Shafer B.A., Dezman L.E., 1982. Development of a Surface Water Supply Index (SWSI) to Assess the Severity of Drought Conditions in Snowpack Runoff Areas. In: Preprints, Western SnowConf., Reno, NV, Colorado State University, pp. 164–175.

Sheffield J., Wood E.F., 2008. Projected changes in drought occurrence under future global warming from multi-model, multi-scenario, IPCC AR4 simulations. *Clim*. *Dyn*., 31(1), 79–105. https://doi.org/10.1007/s00382-007-0340-z.

Shukla S., Wood A.W., 2008. Use of a standardized runoff index for characterizing hydrologic drought. *Geophys*. *Res*. *Lett*., 35(2), L02405. https://doi.org/10.1029/2007GL032487.

Sillmann J, Kharin V.V., Zwiers F.W., Zhang X. and Bronaugh D., 2013. Climate extremes indices in the CMIP5 multimodel ensemble: Part 2. Future climate projections. *J. Geophys. Res. Atmos*., 118, 2473–2493. https://doi.org/10.1002/jgrd.50188.

Sperna Weiland F.C., Van Beek L.P.H., Kwadijk J.C.J., Bierkens M.F.P., 2010. The ability of a GCM-forced hydrological model to reproduce global discharge variability. *Hydrol. Earth Syst. Sci*., 14, 1595–1621. https://doi.org/10.5194/hess-14-1595-2010.

Su B.D., Huang J.L., Zeng X.F., Gao C., Jiang T., 2017. Impacts of climate change on streamflow in the upper Yangtze River basin. *Clim. Change*, 141(3), 533–546. https://doi.org/10.1007/s10584-016-1852-5.

Tallaksen L.M., Hisdal H, van Lanen H.A.J., 2009. Space-time modelling of catchment scale drought characteristics. *J. Hydrol*., 375(3-4), 363–372. https://doi.org/10.1016/j.jhydrol.2009.06.032.

Thibeault J.M., and Seth A., 2014. Changing climate extremes in the Northeast United States: Observations and projections from CMIP5. *Clim. Change*, 127(2), 273–287. https://doi.org/10.1007/s10584-014-1257-2.

Thornton P.K., Ericksen P., Herrero M., Challinor A.J., 2014. Climate variability and vulnerability to climate change: a review. *Global Change Biol*., 20, 3313–3328, https://doi.org/10.1111/gcb.12581.

Touma D., Ashfaq M., Nayak M.A., Kao S.C., Diffenbaugh N.S., 2015. A multi-model and multi-index evaluation of drought characteristics in the 21st century. *J. Hydrol.*, 526, 196–207. https://doi.org/10.1016/j.jhydrol.2014.12.011.

Trenberth K.E., Dai A., Van Der Schrier G., Jones P.D., Barichivich J., Briffa K.R., and Sheffield J., 2014, Global warming and changes in drought, *Nat. Clim. Change*, 4, 17–22, https://doi.org/10.1038/nclimate2067.

Ukkola A.M., Pitman A.J., De Kauwe M.G., Abramowitz G., Herger N., Evans J.P., Decker M., 2018. Evaluating CMIP5 Model Agreement for Multiple Drought Metrics. *J. Hydrometeorol.*, 19(6), 969–988. https://doi.org/10.1175/JHM-D-17-0099.1.

Van Rooy M.P., 1965. A rainfall anomaly index independent of time and space. *Notos*, 14, 43.

van Vuuren D.P., and Coauthors, 2011. The representative concentration pathways: An overview. *Clim. Change*, 109, 5–31. https://doi.org/10.1007/s10584-011-0148-z.

Venkataraman K., Tummuri S., Medina A., Perry J., 2016. 21st century drought outlook for major climate divisions of Texas based on CMIP5 multimodel ensemble: Implications for water resource management. *J. Hydrol.*, 534, 300–316. https://doi.org/10.1016/j.jhydrol.2016.01.001.

Vetter T., Reinhardt J., Flörke M., Griensven A.V., Hattermann F., Huang S.C., et al. 2017. Evaluation of sources of uncertainty in projected hydrological changes under climate change in 12 large-scale river basins. *Clim. Change*, 141(3), 419–433. https://doi.org/10.1007/s10584-016-1794-y.

Vicente-Serrano S.M., Beguería S., López-Moreno J.I., 2010. A multiscalar drought index sensitive to global warming: the standardized precipitation evapotranspiration index. *J. Clim.*, 23(7), 1691–1718. https://doi.org/10.1175/2009JCLI2909.1.

von Buttlar J., Zscheischler J., Ramming A., Sippel S., Reichstein M., Knohl A. et al., 2018. Impacts of droughts and extreme-temperature events on gross primary production and ecosystem respiration: A systematic assessment across ecosystems and climate zones. *Biogeosciences*, 15(5), 1293–1318. https://doi.org/10.5194/bg-15-1293-2018.

Wang G.L., 2005. Agricultural drought in a future climate: results from 15 global climate models participating in the IPCC 4th assessment. *Clim. Dyn.*, 25(7-8), 739–753. https://doi.org/10.1007/s00382-005-0057-9.

Wang L., Chen W., 2014. A CMIP5 multimodel projection of future temperature, precipitation, and climatological drought in China. *Int. J. Climatol.*, 34(6), 2059–2078. https://doi.org/10.1002/joc.3822.

Wang Z.L., Zhong R.D., Lai C.G., Zeng Z.Y., Lian Y.Q., Bai X.Y., 2018. Climate change enhances the severity and variability of drought in the Pearl River Basin in South China in the 21st century. *Agric. For. Meteorol.*, 249, 149–162. https://doi.org/10.1016/j.agrformet.2017.12.077.

Wells, N., Goddard, S., Hayes, M.J., 2004. A self-Calibrating palmer drought severity index. *J. Clim.*, 17(12), 2335–2351. https://doi.org/10.

Wilby R.L. and Harris I., 2006. A framework for assessing uncertainties in climate change impacts: Low-flow scenarios for the River Thames, UK. *Water Resour. Res.*, 42(2), W02419. https://doi.org/10.1029/2005wr004065.

Wilhite D.A., Glantz M.H., 1985. Understanding: the drought phenomenon: the role of definitions. *Water Int.*, 10(3), 111–120. https://doi.org/10.1080/02508068508686328.

Wilhite D.A., 2000. Drought as a natural hazard: concepts and definitions. In: Wilhite D.A.(Ed.), Drought: A Global Assessment, Hazard Disasters Ser, vol. 1. Routledge, New York, USA, pp. 3–18.

World Meteorological Organization (WMO) and Global Water Partnership (GWP) (2016) In tegrated drought management programme handbook of drought indicators and indices. No. 1173. http://www.droughtmanagement.info/literature/GWP_Handbook_of_Drought_Ind icators_and_Indices_2016.pdf.

Woldemeskel F.M., Sharma A., Sivakumar B. & Mehrotra R., 2016. Quantification of precipitation and temperature uncertainties simulated by CMIP3 and CMIP5 models. *J. Geophy. Res. Atmos.*, 121(1), 3–17. https://doi.org/10.1002/2015JD023719.

Wu Z.Y., Lu G.H., Liu Z.Y., Wang J.X., Xiao H., 2013. Trends of extreme flood events in the Pearl River Basin during 1951-2010. 4(2), 110–116. https://doi.org/10.3724SP.J.1248.2013.110.

Wu C.H. & Huang G.R., 2014. Changes in heavy precipitation and floods in the upstream of the Beijiang River basin, South China. *Int. J. Climatol.* 35, 2978–2992. https://doi.org/10.1002/joc.4187.

Wu C.H., Huang G.R., Yu H.J., Chen Z.J., and Ma J.G., 2014. Impact of climate change on reservoir flood control in the upstream area of the Beijiang River Basin, South China. *J. Hydrometeor.*, 15(6), 2203–2218. https://doi.org/10.1175/JHM-D-13-0181.1.

Wu C.H., Huang G.R., and Yu H.J., 2015. Prediction of extreme floods based on CMIP5 climate models: A case study in the Beijiang River basin, South China. *Hydrol. Earth Syst. Sci.*, 19(3), 1385–1399. https://doi.org/10.5194/hess-19-1385-2015.

Wu C.H., Xian Z.Y., Huang G.R., 2016. Meteorological drought in the Beijiang River basin, South China: current observations and future projections. *Stoch. Environ. Res. Risk Assess.*, 30(7), 1821–1834. https://doi.org/10.1007/ s00477-015-1157-7.

Wu C.H. and Huang G.R., 2016. Projection of climate extremes in the Zhujiang River basin using a regional climate model. *Int. J. Climatol.*, 36(3), 1184–1196. https://doi.org/10.1002/joc.4412.

Wu C.H., Yeh Pat J.-F., Chen Y.Y., Hu Bill X., Huang G.R., 2020. Future precipitation-driven meteorological drought changes in the CMIP5 multi-model ensembles under 1.5°C and 2°C global warming. *J. Hydrometeor.*, 21(9), 2177–2196. https://doi.org/10.1175/JHM-D-19-0299.1.

Wu C.H., Yeh P.J.-F, Ju J.L., Chen Y.Y., Xu K., Dai H., Niu J., Hu B.X., and Huang G.R. 2021. Assessing the spatio-temporal uncertainties in future meteorological droughts from CMIP5 models, emission scenarios and bias corrections. *J. Climate*, 34(5), 1903–1922, https://doi: 10.1175/JCLI-D-20-0411.1.

Xiao M.Z., Zhang Q., Singh V.P., Liu L., 2016. Transitional properties of droughts and related impacts of climate indices in the Pearl River basin, China. *J. Hydrol.*, 534, 397–406. https://doi.org/10.1016/j.jhydrol.2016.01.012.

Xu K., Qin G.X., Niu J., Wu C.H., Hu B.X., Huang G.R., and Wang P., 2019a. Comparative analysis of meteorological hydrological drought over the Pearl River basin in southern China. *Hydrol. Res.*, 50(1), 301–318. https://doi.org/10.2166/nh.2018.178.

Xu K., Xu B.B., Ju J.L., Wu C.H., Dai H. and Hu B.X., 2019b. Projection and uncertainty of precipitation extremes in the CMIP5 multimodel ensembles over nine major basins in China. *Atmos. Res.*, 226(15), 122–137. https://doi.org/10.1016/j.atmosres.2019.04.018.

Xu K., Wu C.H. & Hu B.X., 2019c. Projected changes of temperature extremes over nine major basins in China based on the CMIP5 multimodel ensembles. *Stoch. Environ. Res. Risk Assess.*, 33, 321–339. https://doi.org/10.1007/s00477-018-1569-2.

Yan D., Werners S.E., Ludwig F., Huang Q.H., 2015. Hydrological response to climate change: The Pearl River, China under different RCP scenarios. *J. Hydrol. Reg. Stud.*, 4, 228–245. https://doi.org/10.1016/j.ejrh.2015.06.006.

Yang T., Ding J., Liu D., Wang X. & Wang T., 2019. Combined use of multiple drought indices for global assessment of dry gets drier and wet gets wetter paradigm. *J. Clim.*, 32(3), 737– 748. https://doi.org/10.1175/JCLI-D-18-0261.1.

Yao N., Li L.C., Feng P.Y., Feng H., Liu D.L., Liu Y., Jiang K.T., Jiang K.T., Hu X.T., Li Y., 2020. Projections of drought characteristics in China based on a standardized precipitation and evap otranspiration index and multiple GCMs. *Sci. Total Environ.*, 704, 135245. https://doi.org/10.1016/j.scitotenv.2019.135245.

Yoo J.Y., Kwon H.H., Lee J.H. & Kim T.W., 2016. Influence of evapotranspiration on future drought risk using bivariate drought frequency curves. KSCE *J. Civ. Eng.*, 20(5), 2059–2069. https://doi.org/10.1007/ s12205-015-0078-9.

Zarekarizi M., Rana A. & Moradkhani H., 2018. Precipitation extremes and their relation to climatic indices in the Pacific Northwest USA. *Clim. Dyn.*, 50, 4519–4537. https://doi.org/10.1007/s00382-017-3888-2.

Zhang S.R., Lu X.X., Higgitt D.L., Chen C.A., Han J.T., Sun H.G., 2008. Recent changes of water discharge and sediment load in the Zhujiang (Pearl River) Basin, China. *Glob. Planet. Change*, 60(3-4), 365–380. https://doi.org/10.1016/j.gloplacha.2007.04.003.

Zhang Q, Xu C.Y., Zhang Z.X., 2009. Observed changes of drought/wetness episodes in the Pearl River Basin, China, using the Standardized Precipitation Index and Aridity Index. *Theor. Appl. Climatol.*, 98, 89–99. https://doi.org/10.1007/s00704-008-0095-4.

Zhang Q., Xiao M.Z., Singh V.P., Li J.F., 2012. Regionalization and spatial changing properties of droughts across the Pearl River basin, China. *J. Hydrol.*, 472-473, 355–366. https://doi.org/10.1016/j.jhydrol.2012.09.054.

Zhang Q., Xiao M.Z., Singh V.P., Chen X.H., 2013a. Copula-based risk evaluation of droughts across the Pearl River basin, China. *Theor. Appl. Climatol.*, 111(1-2), 119–131. https://doi.org/10.1007/s00704-012-0656-4.

Zhang W.J., Jin F.F., Zhao J.X., Qi I., Ren H.L., 2013b. The Possible Influence of a Nonconventional El Niño on the Severe Autumn Drought of 2009 in Southwest China. *J. Clim.*, 26(21). 8392–8405. https://doi.org/10.1175/JCLI-D-12-00851.1.

Zhang Q., Xiao M.Z., Singh, V.P., 2015. Uncertainty evaluation of copula analysis of hydrological droughts in the East River basin, China. *Glob. Planet. Chang.*, 129, 1–9. https://doi.org/10.1016/j.gloplacha.2015.03.001.

Zhao T., Dai A., 2017. Uncertainties in historical changes and future projections of drought. Part II: model-simulated historical and future drought changes. *Clim. Chang.*, 144, 535–548. https://doi.org/10.1007/s10584-016-1742-x.

Zhou B.T., Wen H.Q.Z., Xu Y., and Song C.L., 2014. Projected Changes in Temperature and Precipitation Extremes in China by the CMIP5 Multimodel Ensembles. *J. Clim.*, 27, 659–6611. https://doi.org/10.1175/JCLI-D-13-00761.1.

Zhu Y., Wang W., Singh V.P., Liu Y., 2016. Combined use of meteorological drought indices at multi-time scales for improving hydrological drought detection. *Sci*. *Total Environ*., 571, 1058–1068. https://dx.doi.org/10.1016/j.scitotenv.2016.07.096.

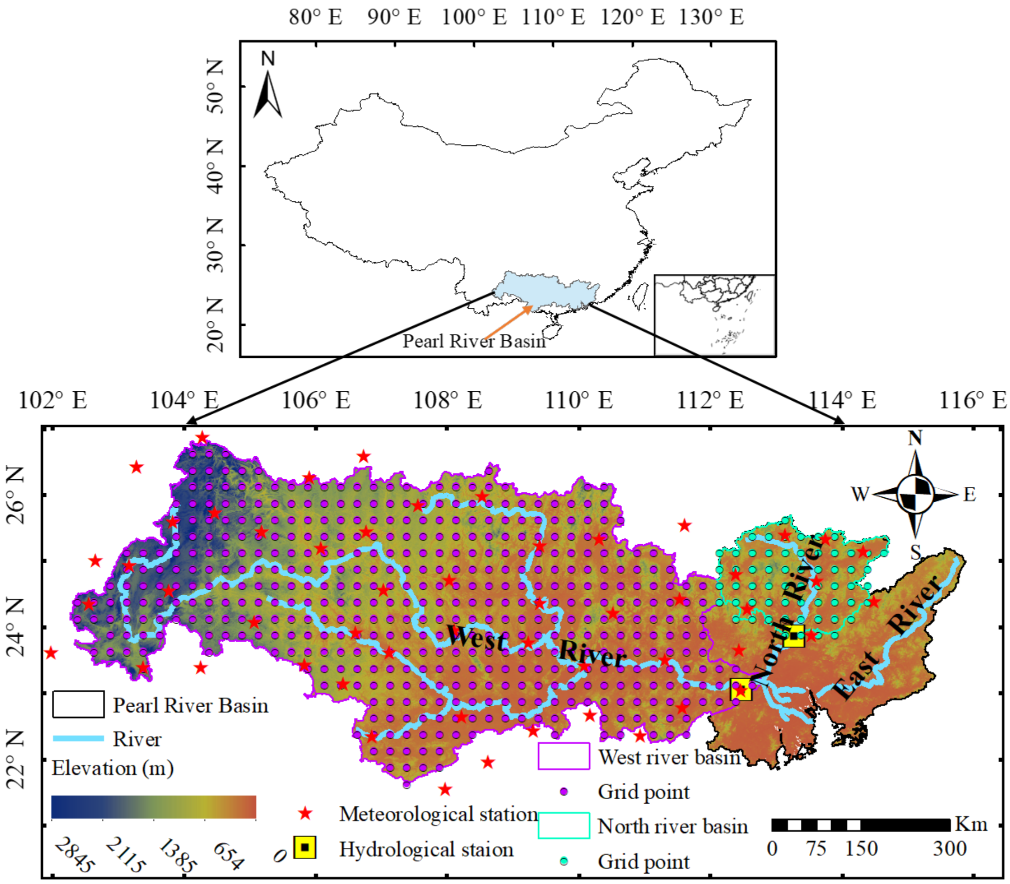

Fig.1. Geographical location map of the Pearl River Basin (PRB) as well as the distributions of 0.25° grid points and meteorological stations.

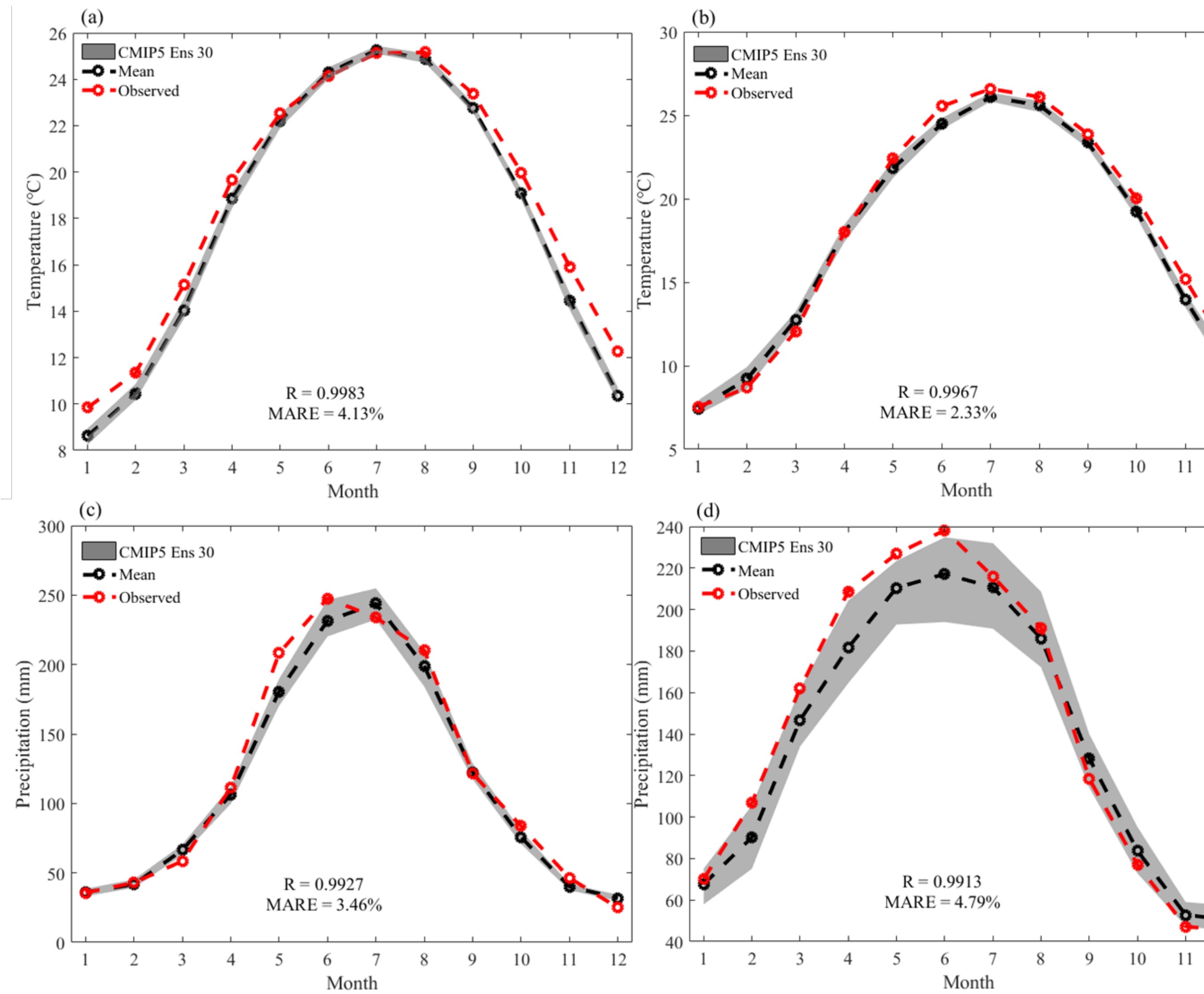

Fig.2. Comparisons of the observed (red dotted line) and bias-corrected (grey shadow) monthly *T* and *P* of 13 CMIP5 GCMs in the West River (a, c) and North River (b, d) basins for the baseline period 1971-2000. The grey shadow represents the range of 30 samples of bias-corrected simulations of the 13 CMIP5 GCMs. *R* and MARE indicate correlation coefficient and mean absolute relatively error, respectively.

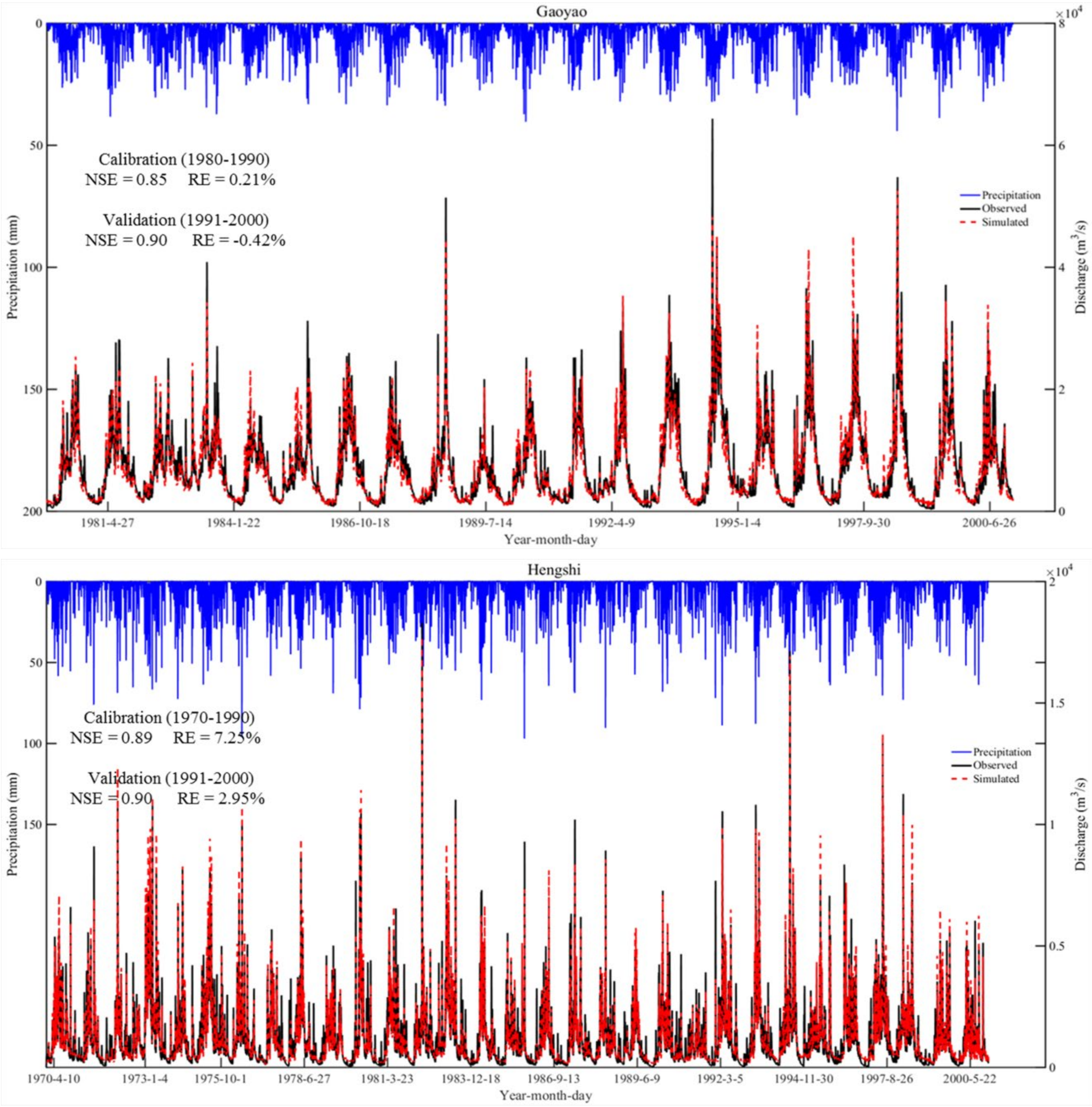

Fig.3. Comparisons of the simulated and observed daily discharges at the Gaoyao (Wet River basin) and Hengshi (North River basin) stations for the calibration and validation periods.

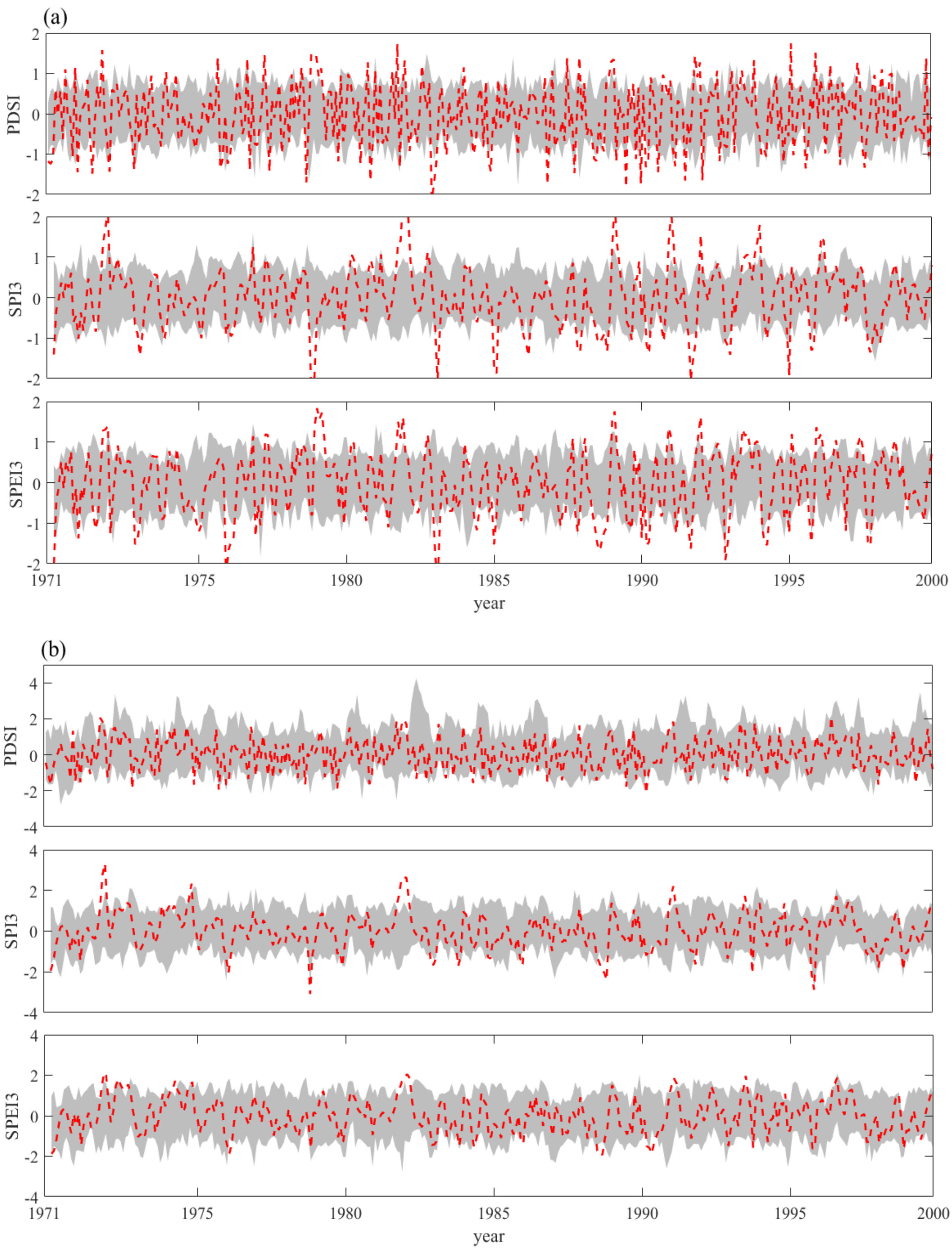

Fig.4. Comparisons of the simulated PDSI, SPI3 and SPEI3 (grey shadow) with the observed ones (red dotted line) in the West River (a) and North River (b) basins during the baseline period 1971-2000. The grey shadow indicates the range of 30 simulation samples of PDSI, SPI3 and SPEI3, and the red dotted lines denotes the observed ones.

1057

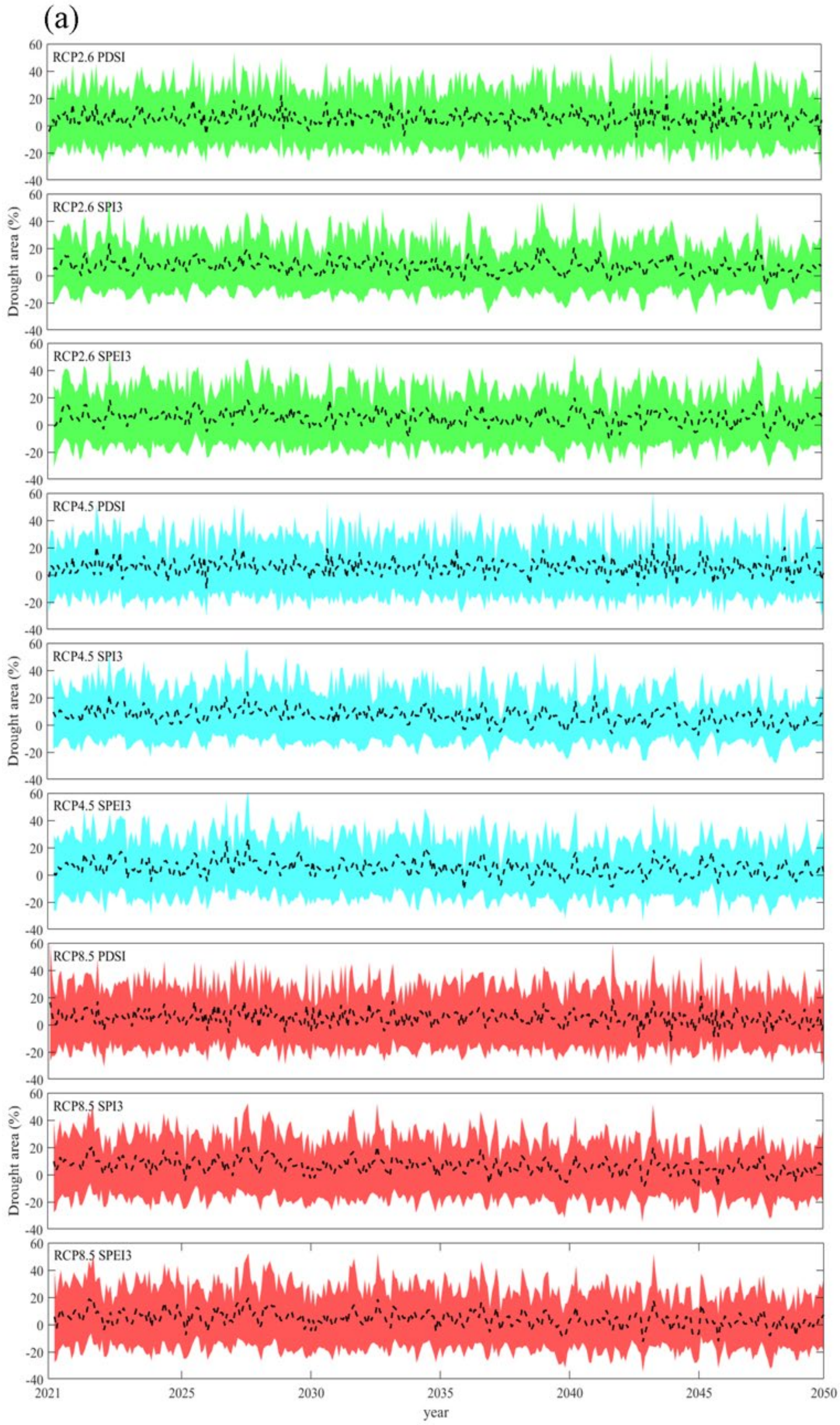

(a)
RCP2.6 PDSI
RCP2.6 SPI3
RCP2.6 SPEI3
RCP4.5 PDSI
RCP4.5 SPI3
RCP4.5 SPEI3
RCP8.5 PDSI
RCP8.5 SPI3
RCP8.5 SPEI3
Drought area (%)
year
2021
2025
2030
2035
2040
2045
2050

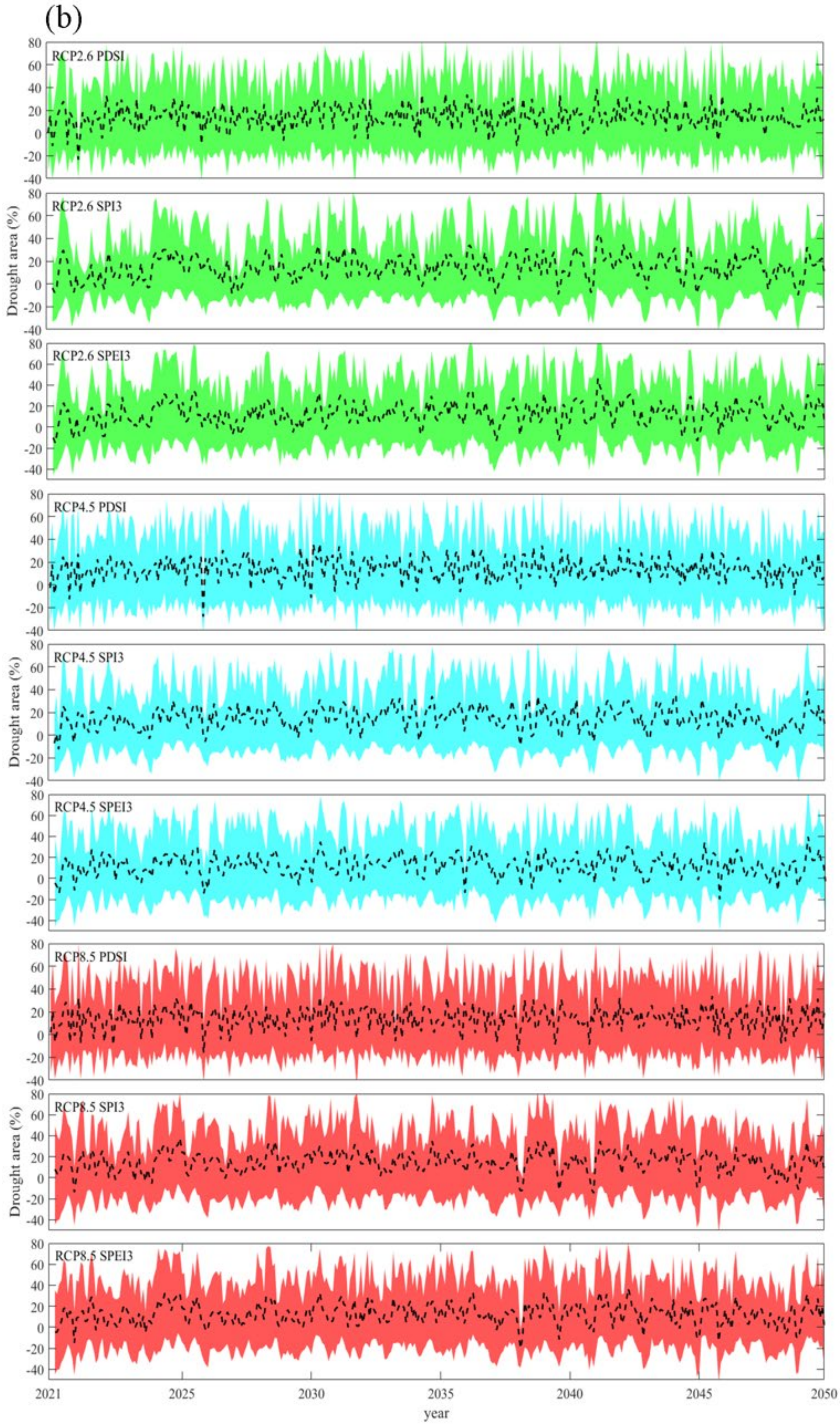

Fig.5. Monthly time series of *Da* (%) indicated by PDSI (≤-1), SPI3 (≤-0.5) and SPEI3 (≤-0.5) under RCP2.6 (green), RCP4.5 (blue) and RCP8.5 (red) scenarios for the future period 2021-2050 (relative to the baseline period 1971-2000) in the West River (a) and North River (b) basins. The shadow denotes the range of 30 simulation of 13 CMIP5 models, and the black lines denotes the ensemble mean of model simulations.

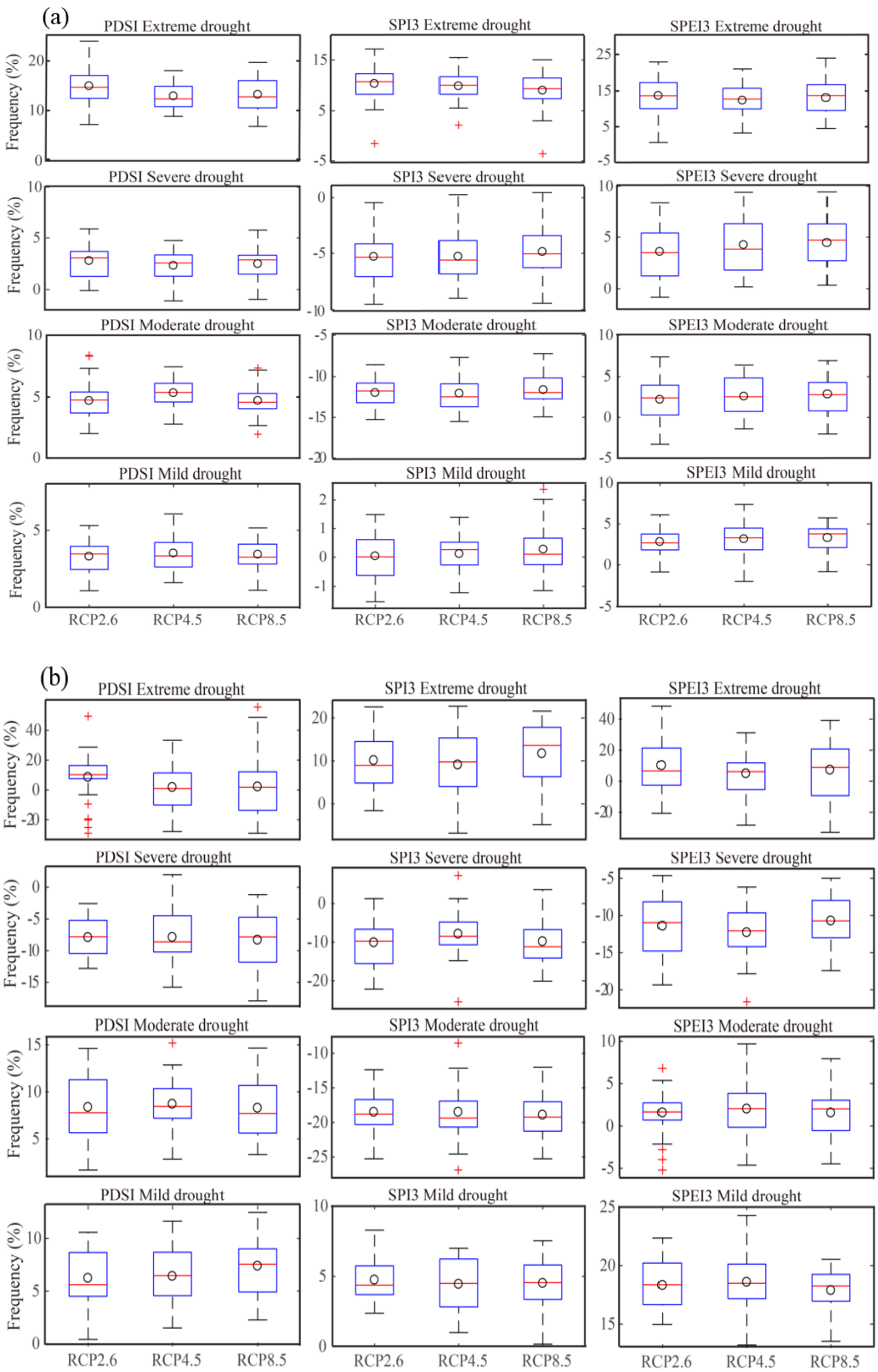

Fig.6. Box plots of relative change (%) in D_F indicated by PDSI (≤-1), SPI3 (≤-0.5) and SPEI3 (≤-0.5) under 3 RCP (RCP2.6, RCP4.5 and RCP8.5) scenarios for the future period 2021-2050 (relative to the baseline period 1971-2000) in the West River (a) and North River (b) basins. Boxes indicate the interquartile model spread (25th and 75th quantiles) with the red horizontal line indicating the ensemble median and the whiskers showing the extreme range of the 30 simulation samples of the 13 CMIP5 GCMs. Black circles denote the average of the multi-model ensembles.

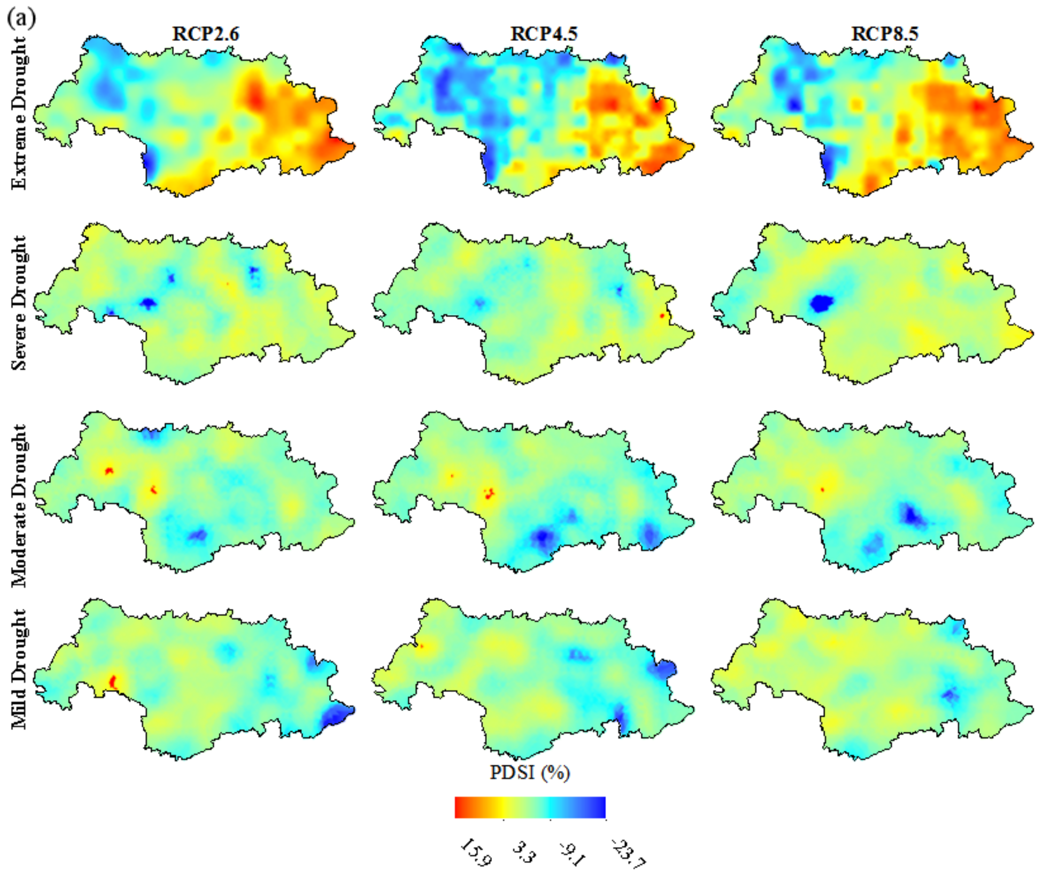
(a)
RCP2.6
RCP4.5
RCP8.5
Extreme Drought
Severe Drought
Moderate Drought
Mild Drought
PDSI (%)
15.9
3.3
-9.1
-23.7

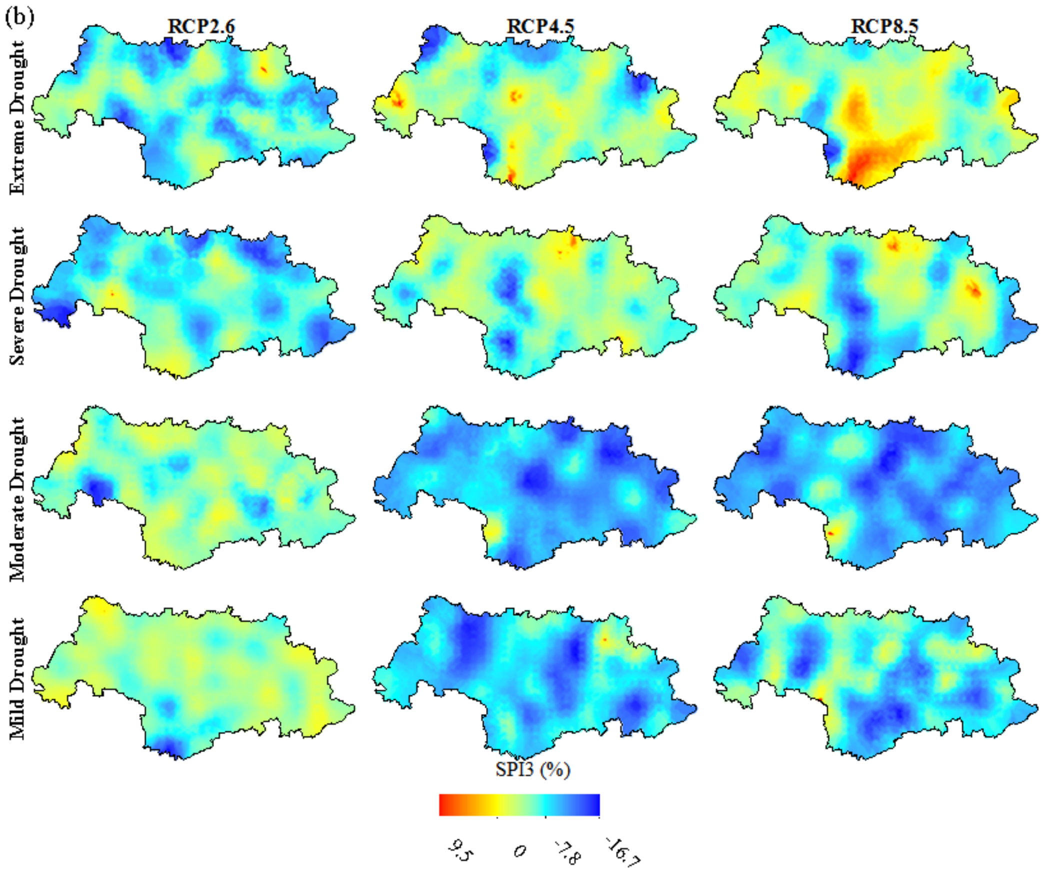
(b)
RCP2.6
RCP4.5
RCP8.5
Extreme Drought
Severe Drought
Moderate Drought
Mild Drought
SPI3 (%)
9.5
0
-7.8
-16.7

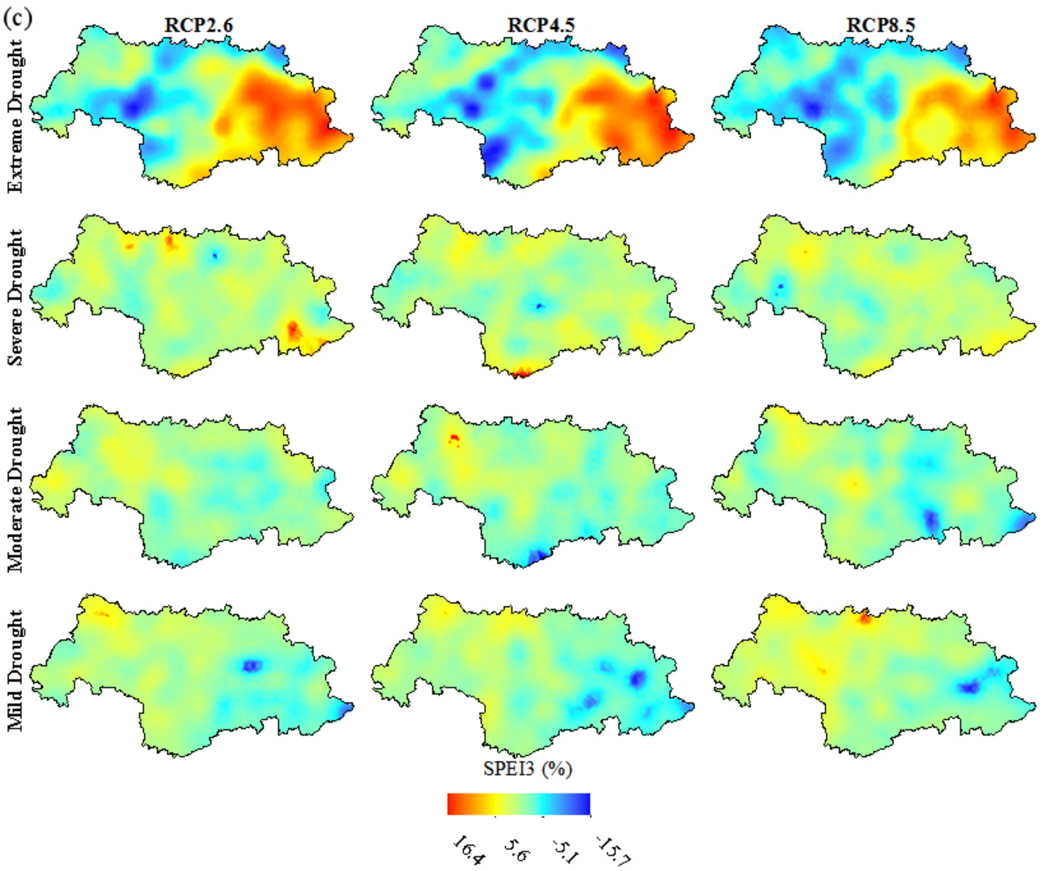

Fig.7. Spatial distributions of D_F (%) indicated by PDSI (a), SPI3 (b) and SPEI3 (c) with extreme, severe, moderate and mild droughts in the future period 2021-2050 (relative to baseline period 1971-2000) under RCP2.6, RCP4.5 and RCP8.5 scenarios in the West River basin.

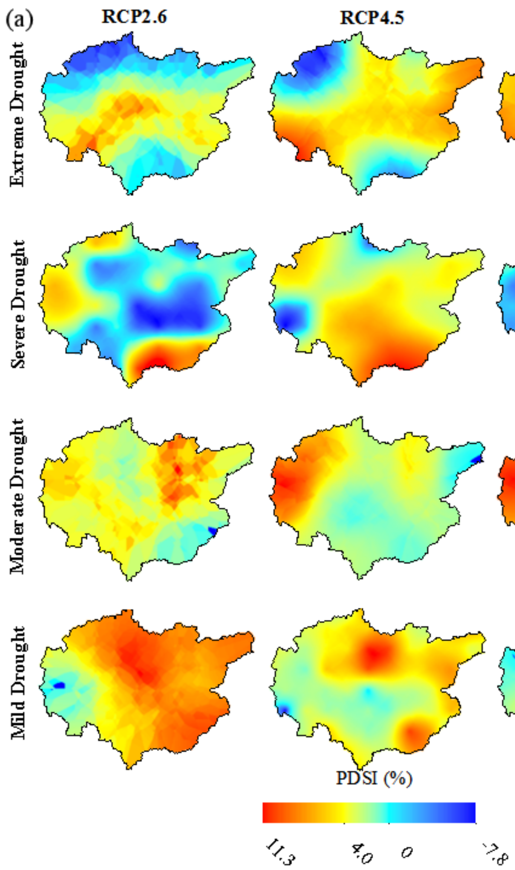
(a)
RCP2.6
RCP4.5
RCP8.5
Extreme Drought
Severe Drought
Moderate Drought
Mild Drought
PDSI (%)
11.3
4.0
0
-7.8

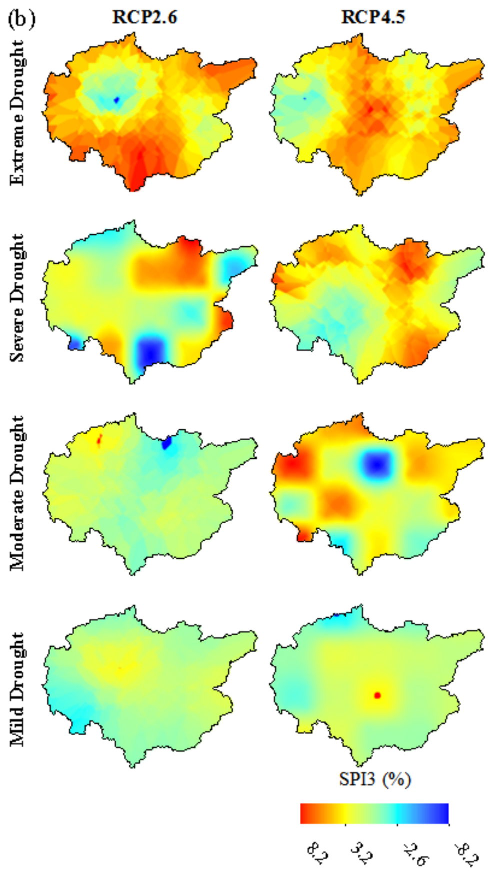
(b)
RCP2.6
RCP4.5
RCP8.5
Extreme Drought
Severe Drought
Moderate Drought
Mild Drought
SPI3 (%)
8.2
3.2
-2.6
-8.2

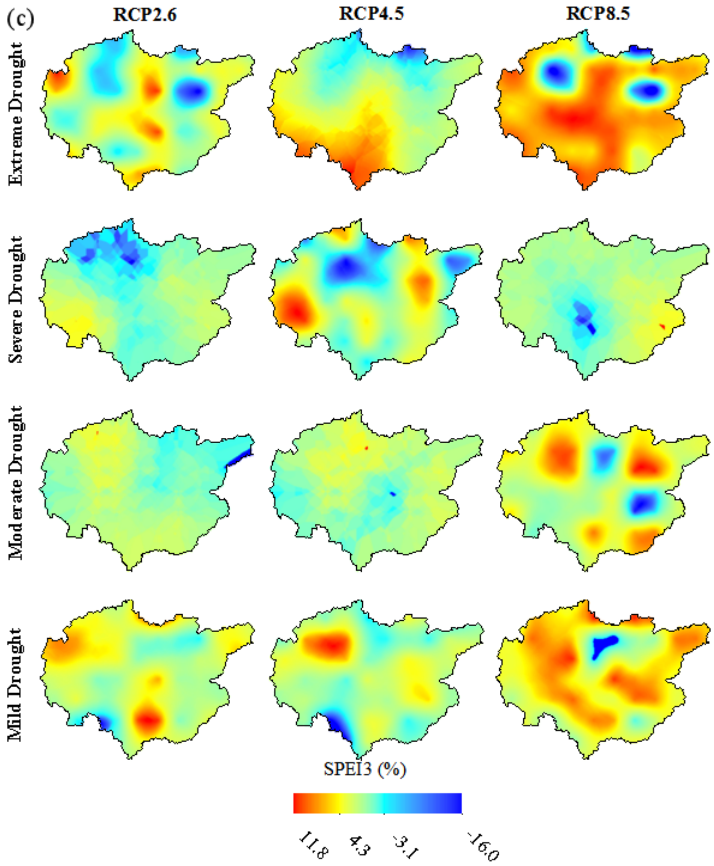

Fig.8. Same as Fig. 7 but for the North River basin.

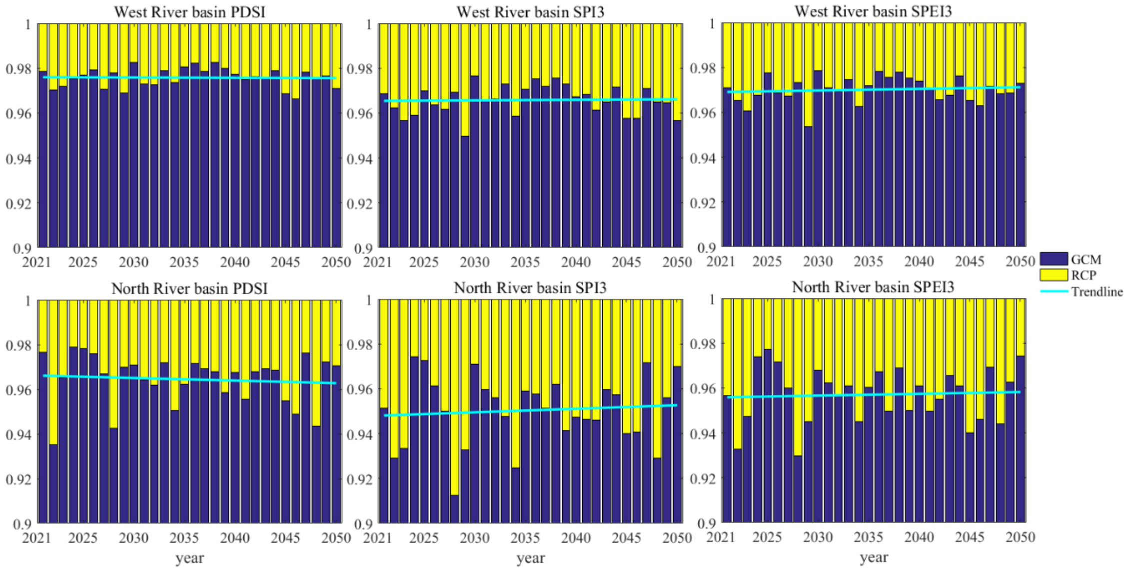

Fig.9. Time series of relative contribution of GCM (blue) and RCP (yellow) to the projection uncertainty of PDSI, SPI3 and SPEI3 in the West and North River basins in the future period 2021-2050. The blue solid line indicates the linear trend of GCM uncertainty.

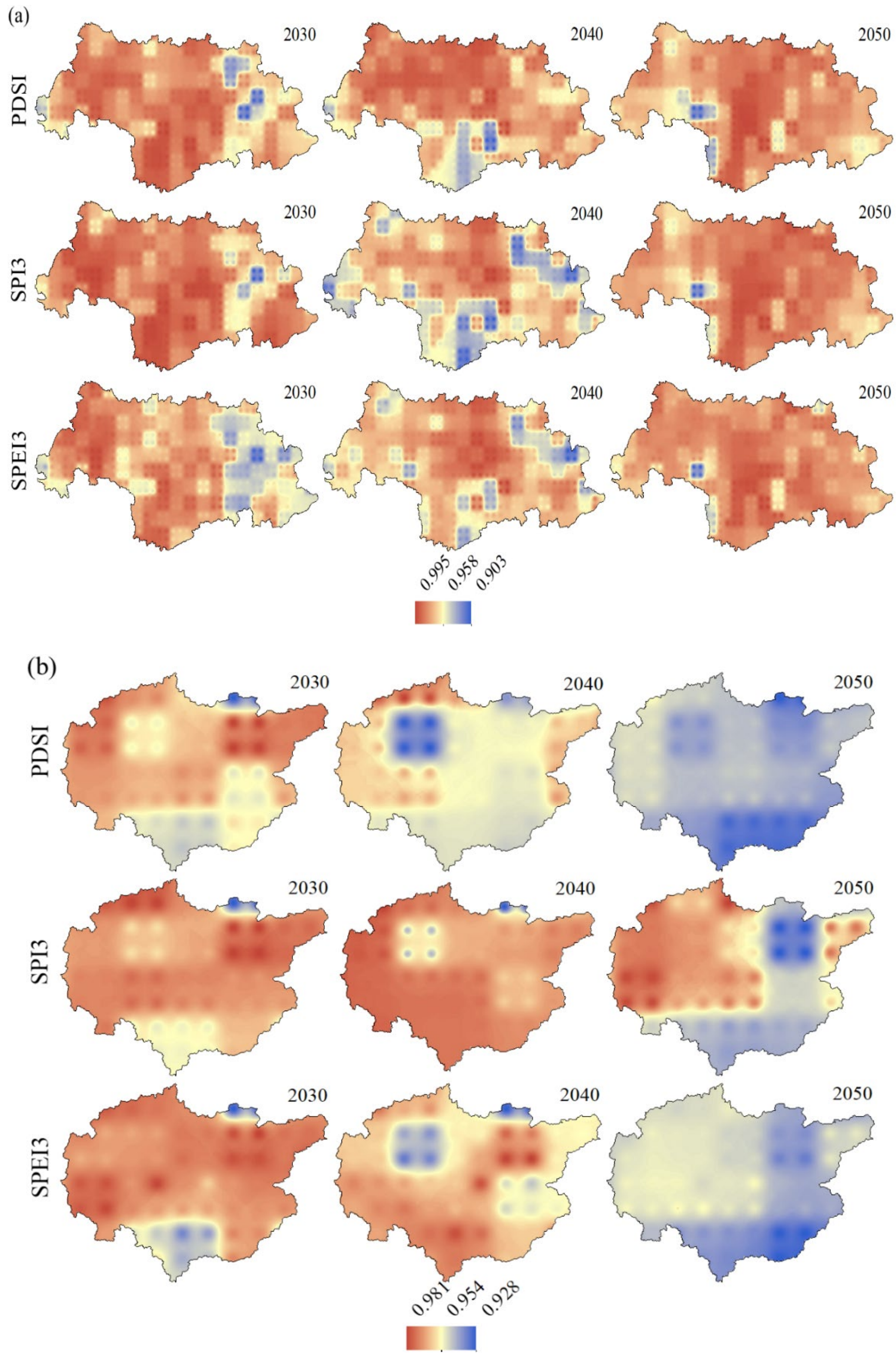

Fig.10. Spatial distributions of the uncertainty contribution GCM to the projections of PDSI, SPI3 and SPEI3 in the West River (a) and North River (b) basins in 2030, 2040 and 2050.

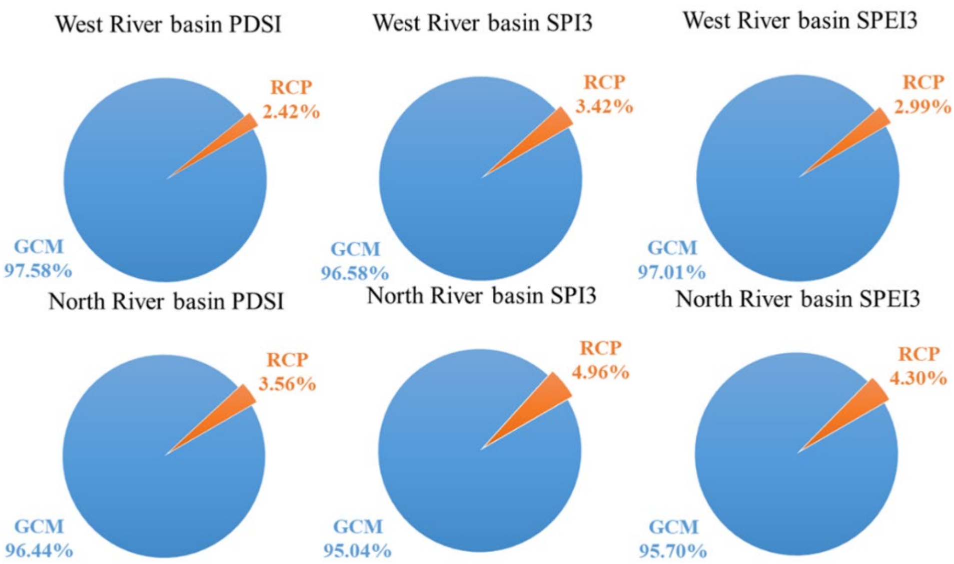

Fig.11. Relative contribution rate (%) of GCM and RCP to the projection uncertainty of PDSI, SPI3 and SPEI3 in the West and North River basins.

Table 1 Information on the 13 general circulation models used in the present analysis

Model	Institution	Country	Resolution
BCC-CSM1.1	Beijing Climate Center (BCC), China Meteorology Administration, China	China	128×64
BNU-ESM	Beijing Climate Center College of Global Change and Earth System Science,Beijing Normal University, China	China	128×64
CNRM-CM5	Centre National de Recherches Meteorologiques and Centre Europeen de Recherches et de Formation Avancee en Calcul Scientifique	France	256×128
GFDL-CM3	National Oceanic and Atmospheric Administration (NOAA) Geophysical Fluid Dynamics Laboratory	America	144×90
GFDL-ESM2G	National Oceanic and Atmospheric Administration (NOAA) Geophysical Fluid Dynamics Laboratory	America	144×90
GISS-E2-R	NASA Goddard Institure for Space Studies	America	144×90
HadGEM2-ES	Met Office Hadley Centre	United Kingdom	192×145
MIROC5	Atmosphere and Ocean Research Institute (The University of Tokyo), National Institute for Environment Studies, and Japan Agency for Marine-Earth Science and Technology	Japan	256×128
MIROC-ESM-CHEM	Japan Agency for Marine-Earth Science and Technology, Atmosphere and Ocean Research Institute (The University of Tokyo), and National Institute for Environment Studies	Japan	128×64
MIROC-ESM	Japan Agency for Marine-Earth Science and Technology, Atmosphere and Ocean Research Institute (The University of Tokyo), and National Institute for Environment Studies	Japan	128×64
MPI-ESM-LR	Max Planck Institute for Meteorology	Germany	192×96
MRI-CGCM3	Meteorological Research Institute	Japan	320×160
NorESM1-M	Norwegian Climate Centre	Norway	144×96

Table 2 Drought Classification based on PDSI, SPI and SPEI

Categories	PDSI classifications	SPI classifications	SPEI classifications
Extremely Drought (Ex_D)	PDSI≤-4.00	SPI≤-2.0	SPEI≤-2.0
Severely Drought (Se_D)	-3.99≤PDSI≤-3.00	-1.99≤SPI≤-1.5	-2.0＜SPEI≤-1.5
Moderately Drought (Mo_D)	-2.99≤PDSI≤-2.00	-1.49≤SPI≤-1.0	-1.5＜SPEI≤-1.0
Mild Drought (Mi_D)	-1.99≤PDSI≤-1.00	-0.99≤SPI≤-0.5	-1.0＜SPEI≤-0.5